

VILNIUS UNIVERSITY
CENTER FOR PHYSICAL SCIENCES AND TECHNOLOGY

Aušrinė
ZABIELAITĖ

Composites of metal nanoparticles for fuel cells

SUMMARY OF DOCTORAL DISSERTATION

Natural sciences,
Chemistry N 003

VILNIUS 2019

This dissertation was written between 2014 and 2018 at the Department of Catalysis of Center for Physical Sciences and Technology. The research was supported by Research Council of Lithuania.

Academic supervisor:

Dr. Loreta Tamašauskaitė (Center for Physical Sciences and Technology, Natural Sciences, Chemistry, N 003)

This doctoral dissertation will be defended in a public meeting of the Dissertation Defence Panel:

Chairman – Prof. Habil. Dr. Albertas Malinauskas (Center for Physical Sciences and Technology, Natural Sciences, Chemistry, N 003).

Members:

Prof. Dr. Ingrida Ancutienė (Kaunas University of Technology, Natural Sciences, Chemistry, N 003).

Prof. Dr. Aldona Beganskienė (Vilnius University, Natural Sciences, Chemistry, N 003).

Prof. Habil, Dr. Rimantas Ramanauskas (Center for Physical Sciences and Technology, Natural sciences, Chemistry, N 003).

Dr. Jolanta Rousseau (France Artois University, Natural Sciences, Chemistry, N 003).

The dissertation shall be defended at a public meeting of the Dissertation Defence Panel at 2 p.m. on 27th September 2019 in Auditorium of the National Center for Physical Sciences and Technology.

Address: Saulėtekio ave. 3, LT-10257 Vilnius, Lithuania

The text of this dissertation can be accessed at the libraries of Center for Physical Sciences and Technology and Vilnius University, as well as on the website of Vilnius University: www.vu.lt/lt/naujienos/ivykiu-kalendorius

VILNIAUS UNIVERSITETAS
FIZINIŲ IR TECHNOLOGIJOS MOKSLŲ CENTRAS

Aušrinė
ZABIELAITĖ

Metalų nanodalelių kompozitai kuro elementams

DAKTARO DISERTACIJOS SANTRAUKA

Gamtos mokslai,
Chemija N 003

VILNIUS 2019

Disertacija rengta 2014–2018 metais Fizinių ir technologijos mokslų centre Katalizės skyriuje. Mokslinius tyrimus rėmė Lietuvos mokslo taryba.

Mokslinis vadovas:

Dr. Loreta Tamašauskaitė Tamašiūnaitė (Fizinių ir technologijos mokslų centras, gamtos mokslai, chemija, N 003)

Gynimo taryba:

Pirmininkas – **prof. habil. dr. Albertas Malinauskas** (Fizinių ir technologijos mokslų centras, gamtos mokslai, chemija, N 003)

Nariai:

prof. dr. Ingrida Ancutienė (Kauno technologijos universitetas, gamtos mokslai, chemija, N 003)

prof. dr. Aldona Beganskienė (Vilniaus universitetas, gamtos mokslai, chemija, N 003)

prof. habil. dr. Rimantas Ramanauskas (Fizinių ir technologijos mokslų centras, gamtos mokslai, chemija, N 003)

dr. Jolanta Rousseau (Prancūzijos Artois universitetas, gamtos mokslai, chemija, N 003)

Disertacija ginama viešame Gynimo tarybos posėdyje 2019 m. rugsėjo mėn. 27 d. 14 val. Nacionalinio fizinių ir technologijos mokslų centro salėje. Adresas: Saulėtekio al. 3, LT–10257 Vilnius, Lietuva

Disertaciją galima peržiūrėti Fizinių ir technologijos mokslų centro ir Vilniaus universiteto bibliotekose ir VU interneto svetainėje adresu:

<https://www.vu.lt/naujienos/ivykiu-kalendoriu>

1. INTRODUCTION

Alternative, renewable energy is currently a relevant and promising area for energy production. One of the cleanest sources of renewable electricity is a fuel cell (FC). New scientific and technological solutions already allow the use of FC prototypes for a wide range of applications. There are built a number of pilot car models operated by electricity produced by fuel cells (Daimler-Crysler, Opel, General Motors, Toyota, Honda). Moreover, the other promising application of fuel cells is power sources for mobile electronic devices (cellular phones, computers, audio-video equipment, etc.) and local power plants for houses, with co-generation of heat (Siemens, Ballard). However, the key disadvantage of FC is their price due to the use of expensive precious metal catalysts. The main precious metals gold (Au) and platinum (Pt), which are used as the anode/cathode materials in FC, are efficient catalysts, but expensive, and this limits their wider use.

This study is related to the preparation of efficient catalysts, their characterization and application as the anode materials for direct borohydride-hydrogen peroxide (DBHPFC) and hydrazine-hydrogen peroxide (DHPFC) fuel cells with the aim to replace expensive noble metals. Moreover, simple and low-cost methods have been used for preparation of catalysts. The ZnCo coating and Co coating having a fiber-like structure have been deposited on the titanium (Ti) or copper (Cu) surfaces using the electrochemical metal deposition method, whereas the latter coatings have been modified with Au or Pt nanoparticles using the galvanic displacement method.

The aim of the work was

Preparation of efficient catalysts, their characterization and application as the anode materials for direct borohydride-hydrogen peroxide and hydrazine-hydrogen peroxide fuel cells.

The main tasks of the work were as follows:

1. Preparation of ZnCo/Ti, AuZnCo/Ti, Co_{fiber}/Ti (Cu), AuCo_{fiber}/Cu and PtCo_{fiber}/Cu catalysts using electrochemical metal deposition and galvanic displacement methods.
2. Characterization of the surface morphology and composition of the fabricated ZnCo/Ti, AuZnCo/Ti, Co_{fiber}/Ti (Cu), AuCo_{fiber}/Cu and PtCo_{fiber}/Cu catalysts using field emission scanning electron microscopy and inductively coupled plasma optical emission spectroscopy.
3. Evaluation of the electrocatalytic activity of ZnCo/Ti, AuZnCo/Ti, Co_{fiber}/Ti(Cu), AuCo_{fiber}/Cu and PtCo_{fiber}/Cu catalysts for the oxidation reactions of sodium borohydride and hydrazine using cyclic voltamperometry and chronoamperometry.
4. Evaluation of the catalytic activity of AuCo_{fiber}/Cu and PtCo_{fiber}/Cu catalysts for the hydrolysis reaction of sodium borohydride.
5. Testing of direct NaBH₄-H₂O₂ and N₂H₄-H₂O₂ fuel cells using the most promising AuCo_{fiber}/Cu and PtCo_{fiber}/Cu catalysts as the anode materials.

Defensive statements:

1. The ZnCo and Co_{fiber} coatings can be deposited on Ti or Cu surfaces using the electrochemical metal deposition method, whereas the ZnCo and Co_{fiber} coatings can be modified with Au or Pt nanoparticles using the galvanic displacement method.
2. The prepared Co_{fiber}/Ti(Cu), ZnCo/Ti, AuZnCo/Ti, AuCo_{fiber}/Cu and PtCo_{pluošt}/Cu catalysts have electrocatalytic activity for the electrooxidation reactions of sodium borohydride and hydrazine. They are suitable for applying them as anode materials in direct NaBH₄-H₂O₂ and N₂H₄-H₂O₂ fuels cells.

3. The electrocatalytic activity of the AuZnCo/Ti catalysts for the oxidation of sodium borohydride and hydrazine is significantly higher than that of the ZnCo/Ti catalyst. The AuCo_{fiber}/Cu and PtCo_{fiber}/Cu catalysts have a higher electrocatalytic activity for the oxidation of sodium borohydride and hydrazine as compared with that of the Co_{fiber}/Cu catalyst.
4. The prepared AuCo_{fiber}/Cu and PtCo_{fiber}/Cu catalysts have catalytic activity for the hydrolysis reaction of NaBH₄. The rate of the hydrogen generation is significantly higher on the Au and Pt nanoparticles modified Co_{fiber} catalyst as compared with that of the pure Co_{fiber} catalyst.

Novelty and actuality of the work

The use of energy from ecological sources (solar, wind and water) to produce electricity has so far not been sufficient to meet the ever-increasing demand for electricity. Therefore, the importance and necessity of renewable electricity sources such as fuel cells have been highlighted in the documents of the World Economic and Energy Forums. Moreover, mobile, renewable power sources are particularly relevant in the field of portable electronics (mobile phones, laptops and tablets, etc.) and in the transport sector. The search of novel efficient catalyst compositions and their application in polymer electrolyte membrane fuel cells (PEMFCs) is industrially vital in order to develop significantly cheaper fuel cell production technologies by replacing well-known and expensive Pt or its alloys with non-noble metals or reducing the amount of precious metals in catalysts. In addition, such a research is important from both fundamental and practical aspects in order to better understand the kinetic peculiarities of electrocatalytic reactions, which are occurring in PEMFCs, and to improve the performance of practical fuel cells.

In this study, novel effective materials have been developed using base metal, such as zinc-cobalt and cobalt having a fiber-like

structure compositions and modifying them with small amounts of gold or platinum nanoparticles with the aim to use these materials as the anodes in direct borohydride (DBFC) and hydrazine (DHFC) fuel cells. The methodology for preparation of AuZnCo/Ti, AuCo_{fiber}/Cu and PtCo_{fiber}/Cu catalysts with very small amounts of Au or Pt nanoparticles has been established. In addition, this methodology allows creating of an efficient AuZnCo/Ti, AuCo_{fiber}/Cu and PtCo_{fiber}/Cu catalysts having a significantly higher electrocatalytic activity for the oxidation of sodium borohydride and hydrazine as compared with that of pure ZnCo/Ti or Co_{fiber}/Cu catalysts. The prepared catalysts have been applied as the anode materials in direct NaBH₄-H₂O₂ and N₂H₄-H₂O₂ fuel cell prototypes. Notably, these catalysts exhibit a higher performance than the previously used catalysts in NaBH₄-H₂O₂ and N₂H₄-H₂O₂ fuel cells, therefore, these AuCo_{fiber}/Cu and PtCo_{fiber}/Cu catalysts can be successfully used in those fuel cells as anode materials.

2. EXPERIMENTAL

Chemicals. Ti foil (99.7% purity, 0.127 mm thick), Cu foil (99.7 % purity, 0.5 mm thick), H₂SO₄ (95%), C₂H₅OH (96%), CoSO₄·7H₂O, (99.5%), C₄H₁₂N₂O (N-(2-Hydroxyethyl) ethylenediamine) (99%), HAuCl₄·3H₂O (99.99%), H₂PtCl₆ (99.95%), MgO, H₂O₂ (35%), HCl (35-38%), NaBH₄ (99%), N₂H₄·2H₂O (50-60%), ZnO (98%), and NaOH (99%) were used. All chemicals were of analytical grade. Deionized water with the resistivity of 18.2 MΩ cm⁻¹ was used to prepare all the solutions. A Nafion N117 membrane was purchased from DuPont (Wilmington, DE).

Fabrication of catalysts. ZnCo, Co and Zn coatings were deposited on the Ti or Cu foil plates (1 x 1 cm) via electrodeposition. Prior to deposition of the coatings, the Ti or Cu plates were pretreated with SiC emery paper (grade 2500) and MgO powder, and then pretreated in the diluted H₂SO₄ (1:1 vol) solution at a temperature of 90 °C for 10 s and rinsed with deionized water. Electrodeposition of coatings was performed using a galvanostatic control with a cathode current density of 40 mA cm⁻² for 20 min at a temperature of 20±2°C. The ZnCo coating with the thickness of ~5 μm was electroplated on the Ti surface from the solution containing 0.12 M ZnO + 0.14 M CoSO₄ + 2.5 M NaOH + 0.6 M C₄H₁₂N₂O. Co coatings with the thickness of ~3 μm were deposited from the same electrolyte with the only difference that Zn ions were excluded from the plating bath. For comparison, the Zn coating with the thickness of ~20 μm was electroplated on the titanium surface using the electrolyte containing 0.12 M ZnO + 2.5 M NaOH + 0.6 M C₄H₁₂N₂O.

Au or Pt crystallites were then deposited onto the Co-coated Cu electrodes by the galvanic displacement technique. For the deposition of Au crystallites, the Co electrodes were dipped into a 1 mM HAuCl₄ + 0.1 M HCl solution at a temperature of 25 °C for 30, 60, and 300 s. For the deposition of Pt crystallites, the Co electrodes

were dipped into a 1 mM H_2PtCl_6 + 0.1 M HCl solution at 25 °C for 10, 30, and 60 s.

Characterization of catalysts. The surface morphology and composition of the prepared catalysts were characterized using a SEM/FIB workstation Helios Nanolab 650 with an energy dispersive X-ray (EDX) spectrometer INCA Energy 350 X-Max 20.

Au, Pt and Co metal loadings in the prepared catalysts were estimated using an ICP optical emission spectrometer Optima 7000DV (Perkin Elmer).

Electrochemical measurements. A conventional three-electrode electrochemical cell was used for electrochemical measurements. The ZnCo/Ti, AuZnCo/Ti, $\text{Co}_{\text{fiber}}/\text{Ti}(\text{Cu})$, $\text{AuCo}_{\text{fiber}}/\text{Cu}$, or $\text{PtCo}_{\text{fiber}}/\text{Cu}$ catalysts with a geometric area of 2 cm² were employed as working electrode, a Pt sheet was used as a counter electrode and an Ag/AgCl/KCl (3 M KCl) electrode was used as a reference.

All electrochemical measurements were performed with a Metrohm Autolab potentiostat (PGSTAT100) using the Electrochemical Software (Nova 1.6.013). Steady state linear sweep voltammograms were recorded in the 0.05 M NaBH_4 + 1 M MaOH and 0.05 M N_2H_4 + 1 M NaOH solutions at a linear potential scan rate of 10 mV s⁻¹ at a temperature of 25 °C. The chronoamperometric curves for the $\text{Co}_{\text{fiber}}/\text{Ti}$, ZnCo/Ti, AuZnCo/Ti, $\text{AuCo}_{\text{pluoŝt}}/\text{Cu}$ catalysts were recorded at a constant potential values for 2 min. The presented current density values were normalized with respect to the geometric area of catalysts. All solutions were deaerated by argon for 30 min prior to measurements

Kinetic studies of the catalytic hydrolysis of NaBH_4 . The amount of generated hydrogen was measured using a MilliGascounter (Type MGC-1 V3.2 PMMA, Ritter, Germany). In a typical measurement, a reaction solution containing NaBH_4 and NaOH was thermostated in an airtight flask, fitted with an outlet connected to the MilliGascounter for collecting evolved H_2 gas. The $\text{Co}_{\text{fiber}}/\text{Cu}$, $\text{AuCo}_{\text{fiber}}/\text{Cu}$, or $\text{PtCo}_{\text{fiber}}/\text{Cu}$ catalysts were then immersed into the

designated temperature solutions containing 5 wt.% NaBH_4 + 0.4 wt.% NaOH to initiate hydrolysis. The rate of hydrogen generation was measured at different solution temperatures to determine the activation energy.

Fuel cell test experiments. Direct borohydride-hydrogen peroxide (DBHPFC) and hydrazine-hydrogen peroxide (DHPFC) fuel cell tests were carried out by employing the $\text{Co}_{\text{fiber}}/\text{Cu}$, $\text{AuCo}_{\text{fiber}}/\text{Cu}$ and $\text{PtCo}_{\text{fiber}}/\text{Cu}$ catalysts with a geometric area of 2 cm^2 as the anode and a Pt sheet with a geometric area of 6 cm^2 as the cathode. The anolyte was composed of an alkaline mixture of 1 M NaBH_4 + 4 M NaOH or 1 M N_2H_4 + 4 M NaOH and the catholyte containing 5 M H_2O_2 + 1.5 M HCl . A Nafion[®]N117 membrane was used for separation of the anodic and cathodic compartments of the single direct $\text{NaBH}_4\text{-H}_2\text{O}_2$ or $\text{N}_2\text{H}_4\text{-H}_2\text{O}_2$ fuel cells. The active area of membrane was ca. 30 cm^2 . Cell measurements were conducted using a Zennium electrochemical workstation (ZAHNER-Elektrik GmbH & Co. KG). The performance of the fuel cell was evaluated by recording the cell polarization at a temperature of $25 \text{ }^\circ\text{C}$ and obtaining the corresponding power density curves.

3. RESULTS AND DISCUSSIONS

3.1 Characterization of catalysts

In this study the ZnCo/Ti, AuZnCo/Ti, Co_{fiber}/Ti, AuCo_{fiber}/Cu and PtCo_{fiber}/Cu catalysts were prepared using electrochemical metal deposition and galvanic displacement methods. Figure 1 shows SEM images of the ZnCo (a), Co_{fiber} (b) and Zn (c) coatings electrodeposited on the Ti surface. As shown in Fig. 1a, the ZnCo coating fully covers the Ti surface and produces a layer of granular Zn and Co particles ca. 0.5-2.5 μm in size. A Co coating that have a fiber-like structure was electrodeposited on the Ti surface with the fibers in the order of tens of nanometers in thickness and hundreds of nanometers in length (Fig. 1b). The layer of polycrystalline Zn with the average size of crystallites ca. 5-14 μm was deposited onto the Ti surface (Fig. 1c). Immersion of the ZnCo/Ti electrodes into the Au(III)-containing solution for various time periods resulted in the deposition of Au nanoparticles on the respective ZnCo coating surface (Fig. 1d-f). As clearly seen, the Au nanoparticles appear as bright, cubic-shaped crystallites, which are homogeneously dispersed on the ZnCo surface (Fig. 1d-f). After immersion of the ZnCo/Ti electrode into the Au(III)-containing solution for 30 and 60 s, Au crystallites sized ca. 10 to 50 nm were deposited on the ZnCo/Ti surface (Fig. 1d, e), while immersion of the ZnCo/Ti electrode into the Au(III)-containing solution for 300 s resulted in the development of larger Au crystallites on the ZnCo coating surface sized in the range of ca. 50 - 200 nm (Fig. 1f).

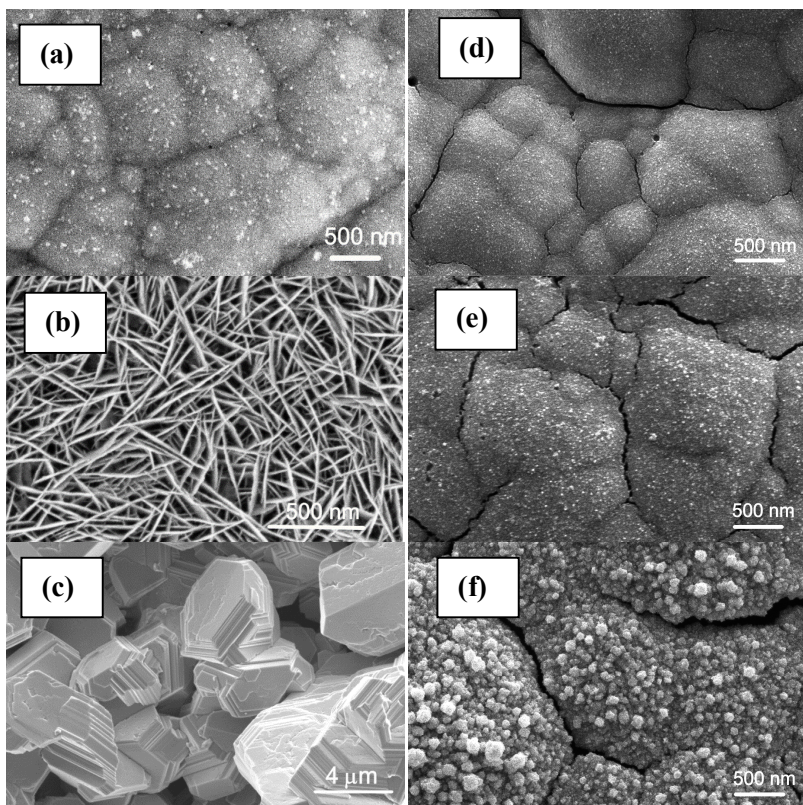


Figure 1. SEM images of the ZnCo/Ti (a), Co_{fiber}/Ti (b), Zn/Ti (c) and AuZnCo/Ti (d-f) catalysts. The AuZnCo/Ti catalysts were prepared by their immersion into the 1 mM HAuCl₄ + 0.1 M HCl solution at 25 °C for 30 (d), 60 (e) and 300 (f) s.

The samples differ from each other in terms of average particle size, interparticle distance and extent of agglomeration. Although the Au particles are hardly discernible in Figs. 1d and e, their residence on the surface of the coating is confirmed by EDX analysis data and are summarized in Table 1. A significant amount of Zn and much lower amounts of Au and Co were determined on the surfaces of ZnCo/Ti and AuZnCo/Ti catalysts. As follows from the

data in Table 1, the increase in the modification time of the ZnCo coating by Au nanoparticles leads to a higher amount of Au on the surface of the catalyst. The amounts of Au loadings on the fabricated catalysts were estimated to be 31, 63 and 306 $\mu\text{g cm}^{-2}$ corresponding to immersion times of 30, 60 and 300 s.

Table 1. Surface atomic composition of the surface of the $\text{Co}_{\text{fiber}}/\text{Ti}$, ZnCo/Ti and AuZnCo/Ti catalysts by EDX analysis. The Au loading was estimated by ICP-OES.

Catalyst	Element, at. %						Au loading, $\mu\text{g cm}^{-2}$
	$t_{\text{Au dep.}}$, S	Au	Zn	Co	O	Ti	
$\text{Co}_{\text{fiber}}/\text{Ti}$	–	–	–	76.32	22.4	1.25	–
ZnCo/Ti	–	–	77.92	18.73	3.21	0.15	–
AuZnCo/Ti	30	0.81	74.71	19.27	5.00	0.21	31.00
AuZnCo/Ti	60	1.49	74.62	19.09	4.54	0.27	63.00
AuZnCo/Ti	300	11.09	38.29	34.87	15.15	0.60	306.00

Figure 2 shows SEM images of the $\text{Co}_{\text{fiber}}/\text{Cu}$ modified with Au (a-c) and Pt (d-f) crystallites. Immersion of the $\text{Co}_{\text{fiber}}/\text{Cu}$ electrodes into the 1 mM $\text{HAuCl}_4 + 0.1 \text{ M HCl}$ or 1 mM $\text{H}_2\text{PtCl}_6 + 0.1 \text{ M HCl}$ solutions for various time periods resulted in the deposition of Au and Pt crystallites on the respective fiber-shaped Co surfaces. EDX analysis data of the prepared $\text{Co}_{\text{fiber}}/\text{Cu}$, $\text{AuCo}_{\text{fiber}}/\text{Cu}$ and $\text{PtCo}_{\text{fiber}}/\text{Cu}$ catalysts are summarized in Tables 2 and 3. The Au and Pt loadings on the catalysts were determined by ICP-OES.

As evident in Fig. 2, the Au nanoparticles appear as bright, cubic-shaped crystallites and are homogeneously dispersed on the fiber-shaped Co surface (Fig. 2, a-c).

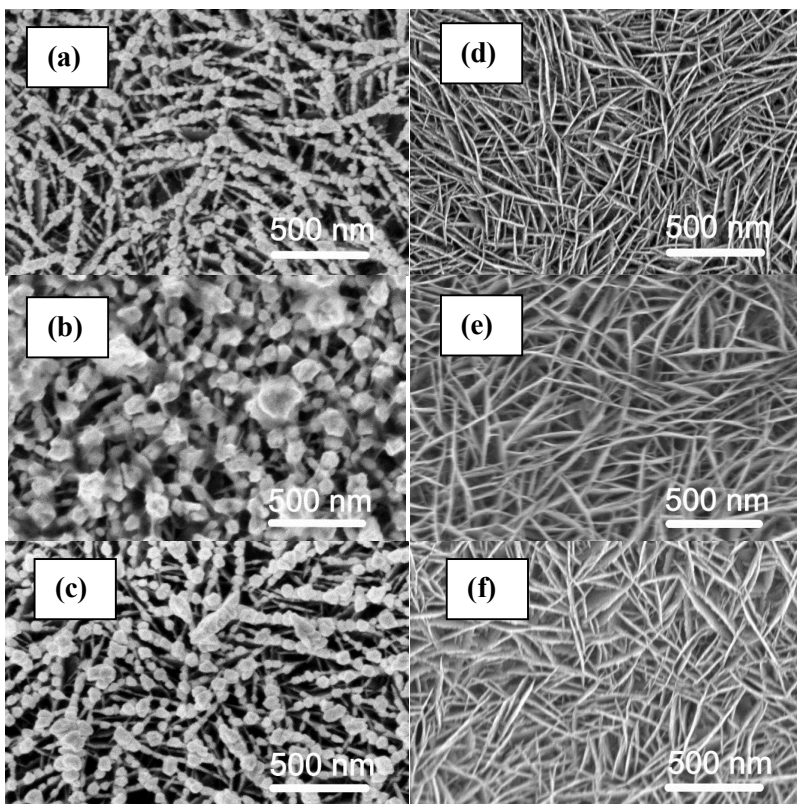


Figure 2. SEM views of the AuCo_{fiber}/Cu (a-c) and PtCo_{fiber}/Cu (d-f) catalysts. The AuCo_{fiber}/Cu catalysts were prepared by immersion of Co_{fiber}/Cu into 1 mM HAuCl₄ + 0.1 M HCl for 30 (a), 60 (b) and 300 (c) s, whereas the PtCo_{fiber}/Cu catalysts were prepared by immersion of Co_{fiber}/Cu into 1 mM H₂PtCl₆ + 0.1 M HCl for 10 (d), 30 (e) and 60 (f) s.

After immersion of the Co_{fiber}/Cu electrode into the 1 mM HAuCl₄ + 0.1 M HCl solution for 30 and 60 s, Au crystallites sized 15 to 50 nm were deposited on the Co_{fiber}/Cu surface (Fig. 2 a,b).

Table 2. Surface atomic composition of the $\text{Co}_{\text{fiber}}/\text{Cu}$ and $\text{AuCo}_{\text{fiber}}/\text{Cu}$ catalysts by EDX analysis. The Au loading was estimated by ICP-OES.

Catalyst	Element, at. %				Au loading, $\mu\text{g cm}^{-2}$
	t_{Audep} , s	Au	Co	Cu	
$\text{Co}_{\text{fiber}}/\text{Cu}$	–	–	99.56	0.43	–
$\text{AuCo}_{\text{fiber}}/\text{Cu}$	30	5.32	94.18	0.50	20.00
$\text{AuCo}_{\text{fiber}}/\text{Cu}$	60	10.08	88.80	1.12	28.00
$\text{AuCo}_{\text{fiber}}/\text{Cu}$	300	20.38	76.62	3.00	96.00

Table 3. Surface atomic composition of the $\text{PtCo}_{\text{fiber}}/\text{Cu}$ catalysts by EDX analysis. The Pt loading was estimated by ICP-OES.

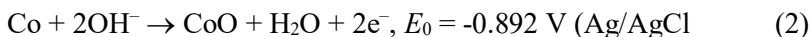
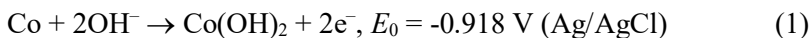
Catalyst	Element, at. %				Pt loading, $\mu\text{g cm}^{-2}$
	t_{Ptdep} , s	Pt	Co	Cu	
$\text{PtCo}_{\text{fiber}}/\text{Cu}$	10	0.67	98.23	1.10	5.4
$\text{PtCo}_{\text{fiber}}/\text{Cu}$	30	1.81	97.50	0.69	15.4
$\text{PtCo}_{\text{fiber}}/\text{Cu}$	60	2.42	95.89	1.70	28.7

Immersion of the $\text{Co}_{\text{fiber}}/\text{Cu}$ electrode into the 1 mM HAuCl_4 + 0.1 M HCl solution for 300 s resulted in the deposition of larger Au crystallites sized 30-100 nm (Fig. 2 c). The amounts of Au loadings on the catalysts were determined to be 20, 28, and 96 $\mu\text{g cm}^{-2}$ corresponding to immersion times of 30, 60 and 300 s (Table 2). In the case of $\text{PtCo}_{\text{fiber}}/\text{Cu}$ catalysts, Pt crystallites were not clearly seen in the SEM images (Fig. 2, d-f). However, their presence was confirmed by the results of EDX and ICP-OES analyses. The Pt loadings were 5.4, 15.4, and 28.7 $\mu\text{g cm}^{-2}$ corresponding to immersion times of 10, 30, and 60 s, respectively (Table 3).

3.2. Electrochemical characterization

3.2.1. Investigation of NaBH₄ and N₂H₄ oxidation on Co_{fiber}/Ti, ZnCo/Ti and AuZnCo/Ti catalysts

The electrochemical behavior of the Zn/Ti, Co_{fiber}/Ti, ZnCo/Ti and AuZnCo/Ti catalysts towards the oxidation of NaBH₄ was evaluated in an alkaline medium using the cyclic voltammetry and chronoamperometry. Figure 3 presents cyclic voltammograms (CVs) for the Co_{fiber}/Ti electrode recorded in 1 M NaOH (a) and that containing 0.05 M NaBH₄ (b) solution at a scan rate of 10 mV s⁻¹. As seen from the data in Fig. 3a, anodic peaks A0 at potential values of ca. -0.8 V and cathodic peaks C0 in the reverse scan at ca. -1.0 V are seen in the CVs. Anodic peak A0 is attributed to the formation of cobalt oxide and hydroxide in an alkaline medium according to the following reactions:



Cathodic peaks C0 are related to the reactivation of the oxidized Co surface during the previous anodic scan, e.g., the reduction of Co oxy/hydroxy compounds to the bare metal. It should be noted that during long-term cycling of the Co_{fiber}/Ti electrode in a 1 M NaOH solution, anodic peak A0 is broadened and increased (Fig. 3a). Figure 3b presents CVs of the Co_{fiber}/Ti electrode recorded in a 0.05 M NaBH₄ + 1 M NaOH solution at 10 mV s⁻¹. During the anodic scan, a well-expressed anodic peak A0 at lower potential values and a broad plateau, denoted as the region A, at potential values more positive than -0.6 V up to 0.1 V are observed in the CVs plots for the Co_{fiber}/Ti electrode. It is clearly seen that anodic peaks A0 recorded in an alkaline NaBH₄ solution at Co_{fiber}/Ti are significantly higher as compared to those recorded using the latter catalyst in a NaOH solution.

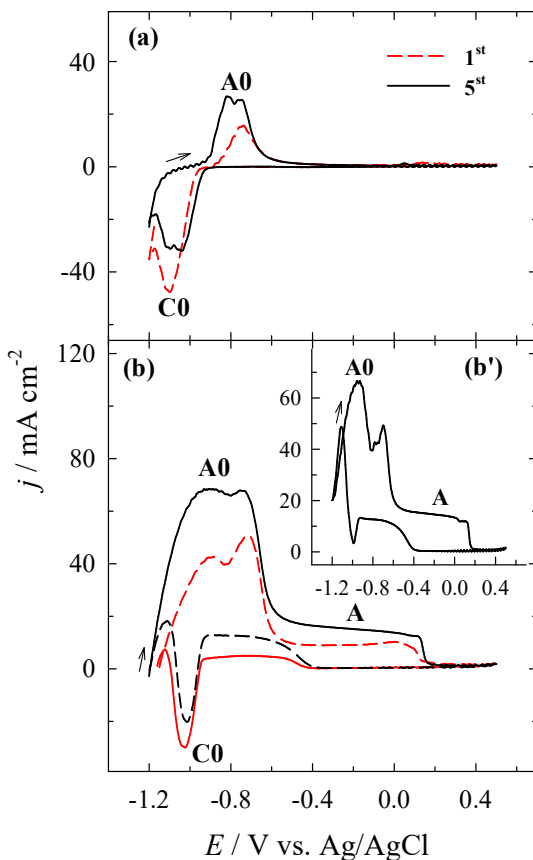


Figure 3. CVs of the $\text{Co}_{\text{fiber}}/\text{Ti}$ catalyst recorded in a 1 M NaOH (a) and that containing 0.05 M NaBH_4 (b) solution at 10 mV s^{-1} ; at $25 \text{ }^\circ\text{C}$. The inset (b') represents the corresponding background corrected data obtained by subtracting the voltammogram of 5th cycle in 0.05 M NaBH_4 + 1 M NaOH by that in 1 M NaOH.

Notably, higher anodic current densities are recorded at $\text{Co}_{\text{fiber}}/\text{Ti}$ in both solutions during long-term cycling (Fig. 3, cf. 1st and 5th cycles), indicating a high activity and stability of the latter catalyst. With the aim to evaluate the behavior of the $\text{Co}_{\text{fiber}}/\text{Ti}$

catalyst in the NaBH₄ solution, the background corrected data are added to Fig. 3b (b', the inset). The background corrected data were obtained by subtracting the voltammogram of 5th cycle in 0.05 M NaBH₄ + 1 M NaOH by that in 1 M NaOH. As seen from the background corrected data in Fig. 3b', well pronounced anodic peak A0 is observed. The anodic peak A0 seen in the CVs for the Co_{fiber}/Ti catalyst is attributed to the oxidation of H₂ generated by the catalytic hydrolysis of NaBH₄ as well as the oxidation of NaBH₄ at more negative potential values.

Figure 4 presents the oxidation of BH₄⁻ ions recorded on the Zn/Ti (a) and ZnCo/Ti (b) electrodes in a 0.05 M NaBH₄ + 1 M NaOH solution at 10 mV s⁻¹. During the anodic scan, an anodic peak A0 at lower potential values and a broad duplet peak A at more positive potential values are seen in the CVs plots for the ZnCo/Ti and Zn/Ti electrodes. Moreover, the anodic peak A0 at Zn/Ti is recorded at more negative potential values as compared to that at Co_{fiber}/Ti and ZnCo/Ti (cfs. Figs. 3b and 4). At higher potential values, the rate of the oxidation of borohydride is diminishing due to the covering of the Zn surface by a layer of Zn oxide. Anodic peak A0 recorded at Zn/Ti at ca. -1.27 V may be attributed to the electro-oxidation of borohydride, while the anodic peak C0 observed in the reverse scan at ca. -1.18 V is related with a reduction of the Zn oxides and consequent reactivation of the electrode surface. In addition, during long-term cycling, the current densities obtained at Zn/Ti in the NaBH₄ solution decreases, indicating dissolution of Zn.

In the case of ZnCo/Ti, anodic peak A0 is seen at a similar potential values as compared with those at Co_{fiber}/Ti and at ca. 0.3 V more positive than that at Zn/Ti (Fig. 4). Anodic current densities (peak A0) recorded at Co_{fiber}/Ti (Fig. 3b) and ZnCo/Ti (Fig. 4b) are close to each other and reach up to 60 mA cm⁻², whereas, the borohydride oxidation current densities (region A) are ~4 and 6 times higher at -0.2 V on the ZnCo/Ti catalysts than those obtained on the Co_{fiber}/Ti and Zn/Ti catalysts.

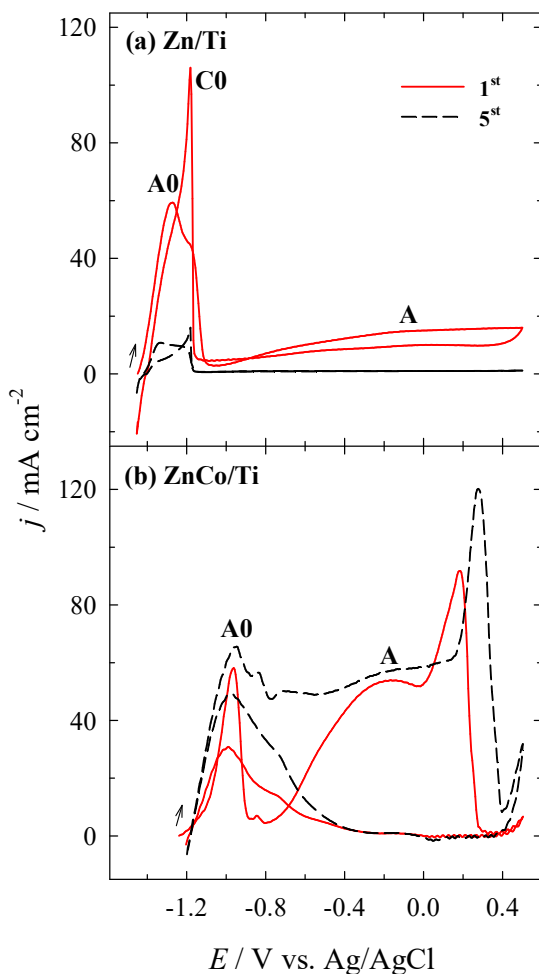


Figure 4. CVs of the Zn/Ti (a) and ZnCo/Ti (b) catalyst recorded in 0.05 M NaBH_4 + 1 M NaOH at 10 mV s^{-1} ; at 25°C

It should be noted that the nature of anodic peak A0 recorded at ZnCo/Ti might be ascribed to the oxidation of H_2 generated by catalytic hydrolysis of NaBH_4 as well as the oxidation of NaBH_4 . Consequently, Zn alloying with Co revealed higher activity of the

ZnCo/Ti catalyst towards NaBH_4 oxidation (region A) as compared with that at Zn/Ti (Fig. 4) and $\text{Co}_{\text{fiber}}/\text{Ti}$ (Fig. 3b).

The stability of the $\text{Co}_{\text{fiber}}/\text{Ti}$ and ZnCo/Ti electrodes for both processes under potential values of peak A0 and region A was investigated under chronoamperometric conditions. Figure 5 presents the corresponding curves for $\text{Co}_{\text{fiber}}/\text{Ti}$ (dashed line) and ZnCo/Ti (solid line), recorded in a 0.05 M NaBH_4 + 1 M NaOH solution at constant potential values of -1.0 (a) and -0.2 (b) V for 130 s. As seen from the data, $\text{Co}_{\text{fiber}}/\text{Ti}$ shows a current decay for both applied potentials. At the end of experimental period ($t = 130$ s), the current densities obtained at -1.0 V are higher than those obtained at -0.2 V. In addition, lower NaBH_4 oxidation current density values at -0.2 V may be related to the passivation of Co electrode caused by the formation of Co hydroxide(s) and oxides in an alkaline medium. Presumably, the surface of catalyst may be poisoned by strongly adsorbed intermediates generated during the oxidation of NaBH_4 and may become inactive for the direct oxidation of NaBH_4 in the reverse scans. In the case of ZnCo/Ti (Fig. 5, solid line), the data obtained also coincide with the data of CV (Fig. 4), showing dissolution of Zn at -1.0 V, whereas at -0.2 V two consecutive electron transfer steps for the oxidation of two oxidizable species. The long-term cyclic voltammograms recorded at ZnCo/Ti are shown in Figure 6. As evident, during the first 10 cycles, current density values under anodic peak A0 and region A remain practically constant, whereas the current densities are decreasing with further potential cycling indicating that the ZnCo/Ti catalyst is not sufficiently stable during the long-term cycling. Degradation of the latter catalyst under continuous cycling of it in a 0.05 M NaBH_4 + 1 M NaOH solution at a scan rate of 10 mV s^{-1} may be related to the simultaneously occurring dissolution of Zn at higher potential values and the changes in the surface structure of Co after disappearing of Zn.

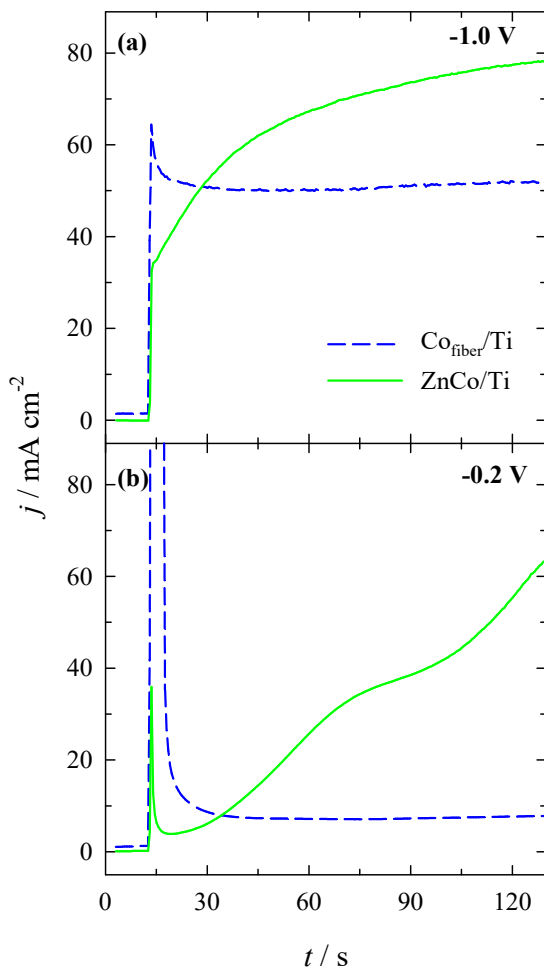


Figure 5. Chronoamperometric data for $\text{Co}_{\text{fiber}}/\text{Ti}$ and ZnCo/Ti recorded in $0.05 \text{ M NaBH}_4 + 1 \text{ M NaOH}$ at constant potential values of -1.0 (a) and -0.2 (b) V for 130 s.

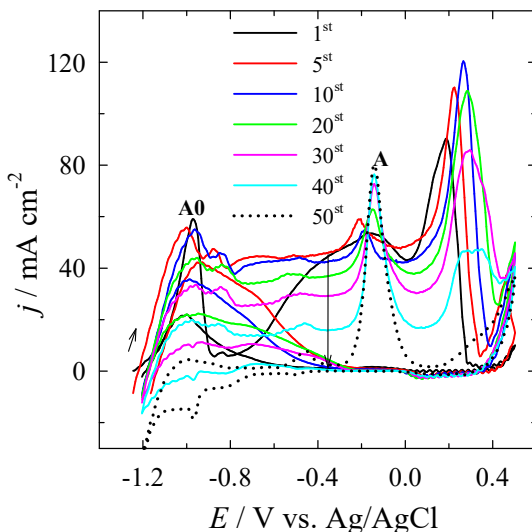


Figure 6. Continuous CVs of ZnCo/Ti recorded in 0.05 M NaBH₄ + 1 M NaOH at 10 mV s⁻¹; at 25 °C.

The comparison of the positive-potential going voltammograms of the oxidation of NaBH₄ recorded on the Zn/Ti (a, *dotted line*), ZnCo/Ti (a, *solid line*) and AuZnCo/Ti (b) catalysts that have the different Au loadings is presented in Fig. 7. As seen from the data obtained in Fig. 7, the oxidation of NaBH₄ proceeds in a more complicated way. During the anodic scan, several well-distinguished anodic peaks are observed in the positive-potential going voltammograms plots. Anodic peaks A0 and A are observed at AuZnCo/Ti under the same potential region as compared with those at ZnCo/Ti (Fig. 7b) and Co_{fiber}/Ti (Fig. 7a), except that the anodic current density values related with the direct oxidation of NaBH₄ (peak A) are enhanced at the ZnCo/Ti modified with Au crystallites.

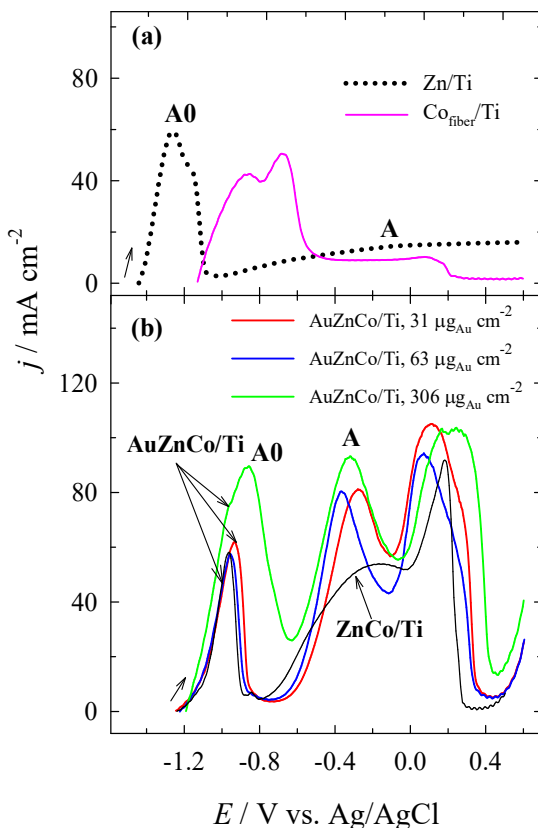


Figure 7. Positive-potential going voltammograms recorded on the Zn/Ti (a), Co/Ti (a), ZnCo/Ti (b), and AuZnCo/Ti (b) catalysts that have Au loadings of 31, 63 and 306 $\mu\text{g}_{\text{Au}} \text{cm}^{-2}$ in 0.05 M NaBH_4 + 1 M NaOH at 10 mV s^{-1} ; at 25°C .

The performance of the investigated $\text{Co}_{\text{fiber}}/\text{Ti}$, ZnCo/Ti and different AuZnCo/Ti catalysts for the oxidation of NaBH_4 (peak A) can be further observed from chronoamperometric measurements. The corresponding chronoamperometric curves recorded at a constant potential value of -0.2 V for 130 s are shown in Fig. 8.

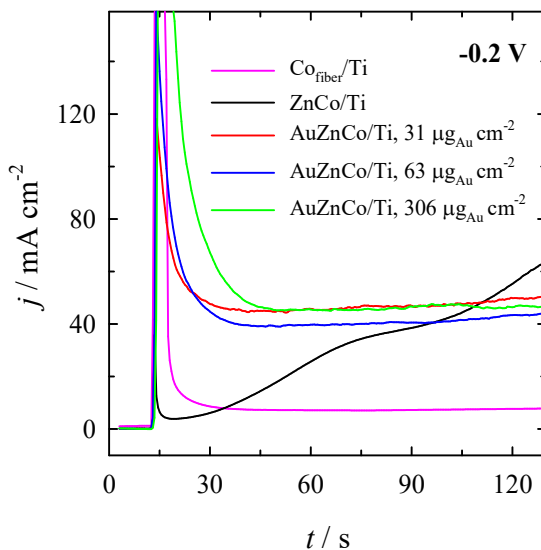


Figure 8. Chronoamperometric data from the $\text{Co}_{\text{fiber}}/\text{Ti}$, ZnCo/Ti and AuZnCo/Ti catalysts that have Au loadings of 31, 63 and $306 \mu\text{g}_{\text{Au}} \text{cm}^{-2}$ at a constant potential value of -0.2 V in $0.05 \text{ M NaBH}_4 + 1 \text{ M NaOH}$. The potential was firstly held at open circuit for 10 s, then set to -0.2 V for 130 s.

The AuZnCo/Ti catalysts that have Au loadings in the range from 31 to $306 \mu\text{g}_{\text{Au}} \text{cm}^{-2}$ and $\text{Co}_{\text{fiber}}/\text{Ti}$ catalysts show a current drop-off for the oxidation of NaBH_4 . At the end of the experimental period ($t = 130 \text{ s}$), the current densities for the all investigated AuZnCo/Ti catalysts are higher than those on pure $\text{Co}_{\text{fiber}}/\text{Ti}$. Moreover, the latter catalysts have a higher catalytic activity and a better stability for the oxidation of NaBH_4 than $\text{Co}_{\text{fiber}}/\text{Ti}$. As seen from the chronoamperogram for ZnCo/Ti (Fig. 8), two consecutive electron transfer steps for the oxidation of two oxidizable species that necessarily are ZnCo alloy and BH_4^- anion. The data obtained are in agreement with the results of cyclic voltammetry.

The electrochemical behavior of the ZnCo/Ti and AuZnCo/Ti catalysts that have different Au loadings towards the oxidation of N_2H_4 was evaluated in an alkaline medium using cyclic voltammetry. Figure 9 presents CVs of the ZnCo/Ti and AuZnCo/Ti catalysts that have Au loadings of 31, 63 and 306 $\mu g\ cm^{-2}$ in the 0.05 M N_2H_4 + 1 M NaOH solution at a scan rate of 10 $mV\ s^{-1}$. The dotted line represents the CV of the ZnCo/Ti catalyst recorded in the 1 M NaOH solution.

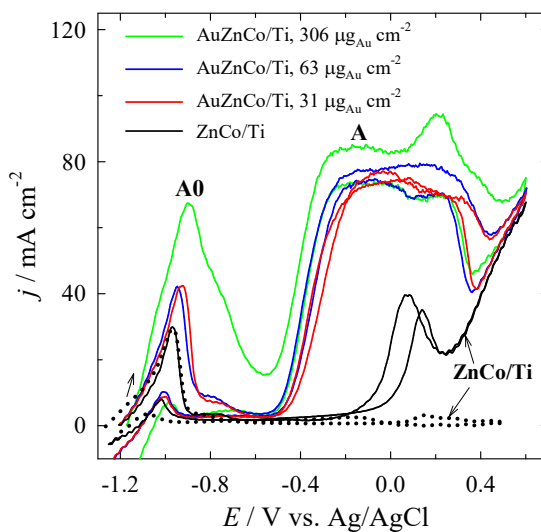


Figure 9. CVs for ZnCo/Ti (*solid line*) and AuZnCo/Ti with the Au loadings of 31, 63 and 306 $\mu g\ cm^{-2}$ recorded in 0.05 M N_2H_4 + 1 M NaOH at 10 $mV\ s^{-1}$; at 25 °C. The dotted line represents the CV of ZnCo/Ti in 1 M NaOH.

During the anodic scan, two well-expressed anodic peaks: peak A0 in the lower potential region and peak A at more positive potential values are seen in the CVs plots for the ZnCo/Ti and AuZnCo/Ti electrodes. Peak A is related to the direct N_2H_4

oxidation. As seen from the data in Fig. 9, ca. 2 times higher current densities under peak A are obtained at the AuZnCo/Ti catalysts that have Au loadings of 31, 63 and 306 $\mu\text{g cm}^{-2}$ as compared to those at ZnCo/Ti. In order to compare the activity of the investigated AuZnCo/Ti catalysts, N_2H_4 oxidation current density values were normalized by Au loadings to represent the mass activity of catalysts. The highest Au-mass activity shows the AuZnCo/Ti catalyst with the lower Au loading of 31 $\mu\text{g cm}^{-2}$ as compared with that at the AuZnCo/Ti catalysts that have higher Au loadings of 63 and 306 $\mu\text{g cm}^{-2}$.

3.2.2. Investigation of NaBH_4 and N_2H_4 oxidation on $\text{Co}_{\text{fiber}}/\text{Cu}$, $\text{PtCo}_{\text{fiber}}/\text{Cu}$ and $\text{AuCo}_{\text{fiber}}/\text{Cu}$ catalysts

The electrocatalytic activity and stability of the $\text{Co}_{\text{fiber}}/\text{Cu}$, $\text{PtCo}_{\text{fiber}}/\text{Cu}$ and $\text{AuCo}_{\text{fiber}}/\text{Cu}$ catalysts have been investigated towards the oxidation of NaBH_4 and N_2H_4 using cyclic voltammetry and chronoamperometry. Figure 10 shows the CVs recorded on the pure $\text{Co}_{\text{fiber}}/\text{Cu}$ catalyst in the background 1 M NaOH solution (dashed line) and that containing 0.05 M NaBH_4 (solid line). As evident from the data in Fig. 10, the electrochemical behavior of $\text{Co}_{\text{fiber}}/\text{Cu}$ catalyst as in the background solution, as in the NaBH_4 solution is the same as for the Co_{fiber} coating deposited on the Ti surface (Fig. 3). A well-expressed anodic peak A0 in the lower potential region and a broad plateau (denoted as the region A) at potential values more positive than -0.6 V up to 0.1 V are observed in the CVs plots for the $\text{Co}_{\text{fiber}}/\text{Cu}$ electrode in the NaBH_4 solution and may be related with the following processes occurring on the electrode surface: formation of Co oxide/hydroxide compounds on the Co surface (1, 2 equations), the oxidation of NaBH_4 and the oxidation of H_2 , generated from the spontaneous hydrolysis of NaBH_4 . Moreover, significantly higher anodic current density values

were obtained on the $\text{Co}_{\text{fiber}}/\text{Cu}$ electrode in the NaBH_4 solution as compared with those in the background solution.

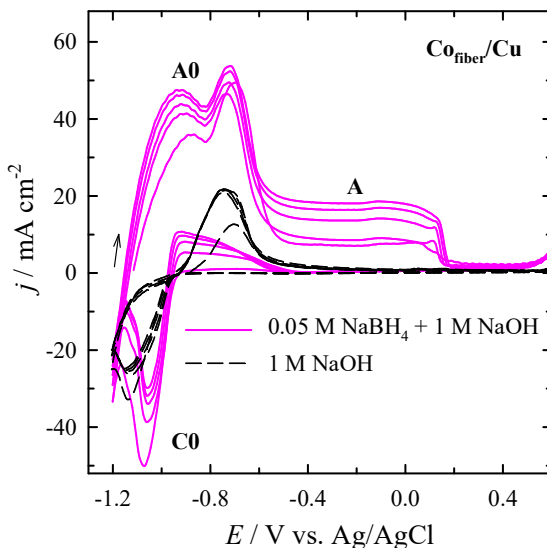


Figure 10. CVs of the $\text{Co}_{\text{fiber}}/\text{Cu}$ catalyst recorded in a 1 M NaOH (dashed line) and that containing 0.05 M NaBH_4 (solid line) solution at 10 mV s^{-1} ; at $25 \text{ }^\circ\text{C}$.

Figure 11 presents comparable positive-going potential stabilized voltammograms (5 cycles) of the oxidation of NaBH_4 recorded for the $\text{Co}_{\text{fiber}}/\text{Cu}$ (a, c), $\text{PtCo}_{\text{fiber}}/\text{Cu}$ (a) and $\text{AuCo}_{\text{fiber}}/\text{Cu}$ (c) catalysts. It is evident that the oxidation of NaBH_4 on the $\text{PtCo}_{\text{fiber}}/\text{Cu}$ and $\text{AuCo}_{\text{fiber}}/\text{Cu}$ catalysts proceeds in a more complicated way. Well-expressed anodic peaks are seen in the CVs plots: one peak A0 at more negative potential values and another one A at more positive potential values.

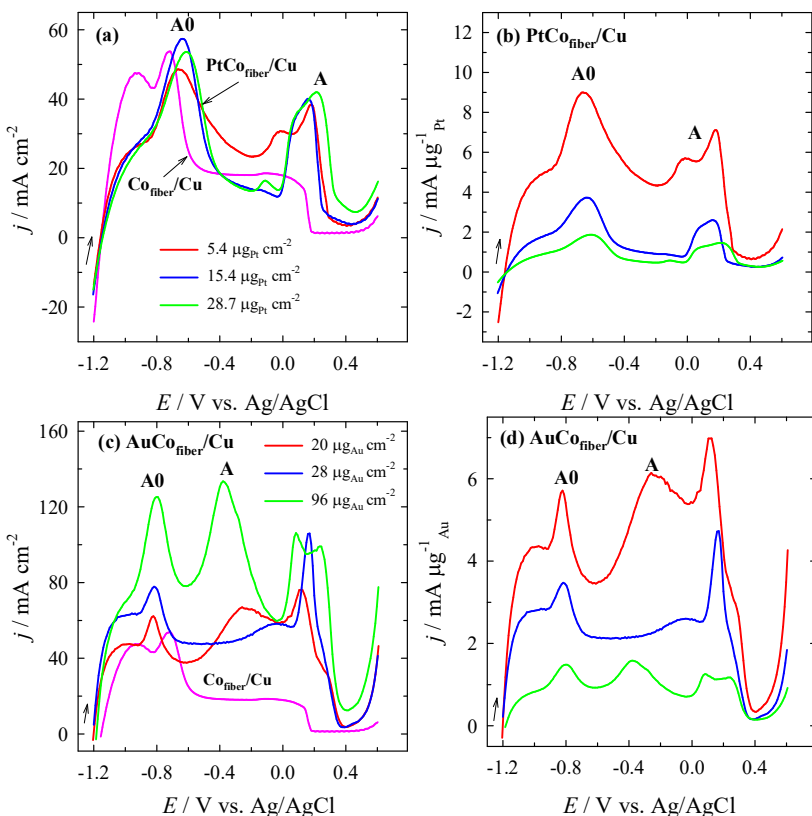


Figure 11. Positive-potential going voltammograms (5 cycles) of the Co_{fiber}/Cu (a, c), $PtCo_{fiber}/Cu$ (a) and $AuCo_{fiber}/Cu$ (c) catalysts recorded in a 0.05 M $NaBH_4$ + 1 M $NaOH$ solution at $10 mV s^{-1}$; at 25 °C. The data were normalized by the Pt (b) and Au (d) loading for each catalyst.

Sodium borohydride oxidation current density values under peak A measured on the $AuCo_{fiber}/Cu$ and $PtCo_{fiber}/Cu$ catalysts are ca. 2 and 4-6, respectively, times higher than those on the pure Co_{fiber}/Cu electrode (Fig. 11a, c). This phenomenon indicates that decoration of pure Co_{fiber}/Cu electrode with low amounts of Au and

Pt nanoparticles results in enhanced activity for the oxidation of NaBH_4 . Therefore, the enhanced electrocatalytic activity of the $\text{AuCo}_{\text{fiber}}/\text{Cu}$ and $\text{PtCo}_{\text{fiber}}/\text{Cu}$ catalysts may be attributed to the synergistic effect between the metals present in the catalyst composition.

In order to compare of the electrocatalytic activity of the prepared $\text{PtCo}_{\text{fiber}}/\text{Cu}$ and $\text{AuCo}_{\text{fiber}}/\text{Cu}$ catalysts, the NaBH_4 oxidation current density values were normalized according to the Pt and Au loading for each catalyst (Fig. 14b, d). It should be noted that the highest mass activity for NaBH_4 oxidation have the $\text{PtCo}_{\text{fiber}}/\text{Cu}$ catalyst that have the Pt loading of $5.4 \mu\text{g cm}^{-2}$ (Fig. 11b) and $\text{AuCo}_{\text{fiber}}/\text{Cu}$ catalyst that have the Au loading of $20 \mu\text{g cm}^{-2}$ (Fig. 11d).

The stability of the prepared $\text{Co}_{\text{fiber}}/\text{Cu}$, $\text{PtCo}_{\text{fiber}}/\text{Cu}$ and $\text{AuCo}_{\text{fiber}}/\text{Cu}$ catalysts has been investigated by chronoamperometry. Figure 12 shows chronoamperograms recorded on the $\text{Co}_{\text{fiber}}/\text{Cu}$ and $\text{PtCo}_{\text{fiber}}/\text{Cu}$ catalysts that have Pt loadings of 5.4, 15.4 or 28.7 $\mu\text{g cm}^{-2}$ in a 0.05 M NaBH_4 + 1 M NaOH solution at a constant potential value of 0.2 V for 1800 s. As seen from the obtained data, the $\text{Co}_{\text{fiber}}/\text{Cu}$ and $\text{PtCo}_{\text{fiber}}/\text{Cu}$ catalysts show a current decay for the oxidation of NaBH_4 . At the end of the experimental period ($t = 1800$ s), the current densities of the $\text{PtCo}_{\text{fiber}}/\text{Cu}$ catalysts are higher than those on $\text{Co}_{\text{fiber}}/\text{Cu}$. Furthermore, current density values normalized by Pt loadings for each catalyst are greater on the $\text{PtCo}_{\text{fiber}}/\text{Cu}$ catalyst that have the lowest Pt loading of $5.4 \mu\text{g cm}^{-2}$.

Figure 13 presents the chronoamperometric data from the $\text{Co}_{\text{fiber}}/\text{Cu}$ and $\text{AuCo}_{\text{fiber}}/\text{Cu}$ catalysts that have Au loadings of 20, 28 and 96 $\mu\text{g cm}^{-2}$ recorded in a 0.05 M NaBH_4 + 1 M NaOH solution at constant potential values of -0.8 V (a) and -0.2 V (b) for 1800 s. As seen from the data in Fig. 13, the $\text{Co}_{\text{fiber}}/\text{Cu}$ and $\text{AuCo}_{\text{fiber}}/\text{Cu}$ catalysts show a current decay for the oxidation of NaBH_4 in both cases.

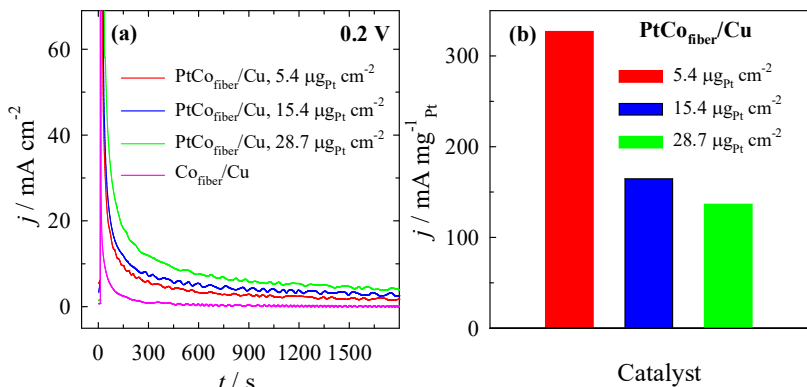


Figure 12. (a) Chronoamperometric data from the Co_{fiber}/Cu and PtCo_{fiber}/Cu catalysts with the Pt loading of 5.4, 15.4 and 28.7 μg cm⁻² recorded at a constant potential value of 0.2 V in a 0.05 M NaBH₄ + 1 M NaOH solution for 1800 s. (b) Bar columns of current density values at 1800 s normalized by Pt loadings for each catalyst.

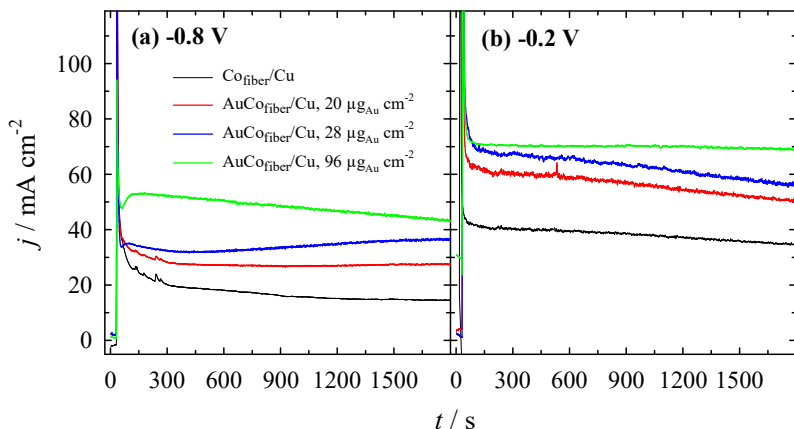


Figure 13. Chronoamperometric data from the Co_{fiber}/Cu and AuCo_{fiber}/Cu catalysts that have Au loadings of 20, 28 or 96 μg cm⁻² recorded at constant potential values of -0.8 V (a) and -0.2 V (b) in a 0.05 M NaBH₄ + 1 M NaOH solution for 1800 s; 25 °C.

At the end of experimental period ($t = 1800$ s), the current densities of the all $\text{AuCo}_{\text{fiber}}/\text{Cu}$ catalysts at -0.8 and -0.2 V are ca. 2-3 and 1.4-2, respectively, times higher than those on $\text{Co}_{\text{fiber}}/\text{Cu}$ (Fig. 13). It was found that the highest mass activity for sodium borohydride oxidation at potential values of -0.8 and -0.2 V has the $\text{AuCo}_{\text{fiber}}/\text{Cu}$ catalyst that have the lowest Au loading of $20 \mu\text{g cm}^{-2}$.

Figure 14a shows comparable positive-going potential stabilized voltammograms (5 cycles) of the oxidation of N_2H_4 recorded for the $\text{Co}_{\text{fiber}}/\text{Cu}$ and different $\text{PtCo}_{\text{fiber}}/\text{Cu}$ catalysts.

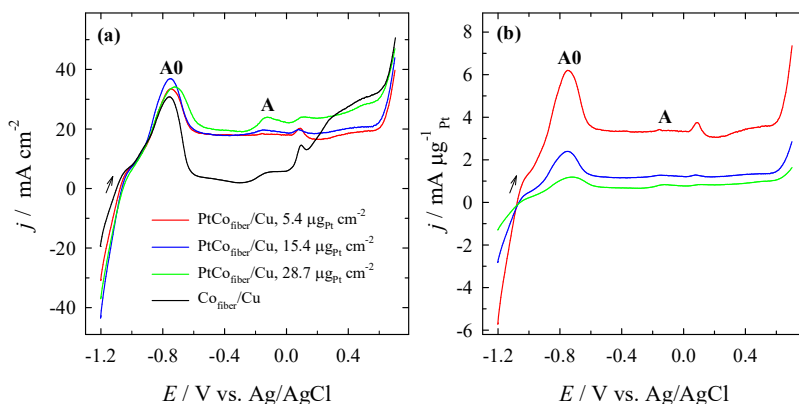


Figure 14. (a) Positive-potential going voltammograms (5 cycles) of the $\text{Co}_{\text{fiber}}/\text{Cu}$ and $\text{PtCo}_{\text{fiber}}/\text{Cu}$ catalysts that have Pt loadings of 5.4, 15.4 and $28.7 \mu\text{g cm}^{-2}$ recorded in a $0.05 \text{ M N}_2\text{H}_4 + 1 \text{ M NaOH}$ solution at 10 mV s^{-1} ; $25 \text{ }^\circ\text{C}$. (b) The data were normalized by the Pt loading for each catalyst.

It is clearly seen that the oxidation process of N_2H_4 is the potential dependent process. A typical current peak in the low potential region (peak A0), followed by a current plateau at higher potential values (region A), which indicates the diffusion-controlled process of the oxidation of N_2H_4 , are seen in the voltammograms (Fig. 14 a). The current densities that correspond to the peak A0 of

the different PtCo_{fiber}/Cu catalysts have similar values. They are, in general, slightly larger compared with that of the Co_{fiber}/Cu catalyst (Fig. 14a). Furthermore, in the potential region between -0.6 V and 0 V (region A), the measured current density values on the PtCo_{fiber}/Cu catalysts significantly outperform those determined on a pure Co_{fiber}/Cu catalyst. The measured N₂H₄ oxidation current density values that correspond to the region A at a potential value of -0.2 V are ca. 5.5, 5.7, and 6.3 times larger at the PtCo_{fiber}/Cu catalysts that have Pt loadings of 5.4, 15.4 and 28.7 μg cm⁻², respectively, compared with those for a pure Co_{fiber}/Cu catalyst (Fig. 14a). Consequently, the enhanced electrocatalytic activity of the PtCo_{fiber}/Cu catalysts may be attributed to the synergistic effect between the metals present in the catalyst composition and the change in Pt electronic structure due to the presence of Co. The N₂H₄ oxidation current density values that correspond to the peak A0 and region A were normalized according to the Pt loadings for each catalyst in order to represent their mass activity towards a hydrazine oxidation (Fig. 14b). The data show that the highest mass activity was obtained for the Co_{fiber}/Cu modified electrode that has the lowest Pt loading of 5.4 μg cm⁻² (Fig. 14b). In addition, approximately 2.6-5.0 and 3.0-4.6 times higher mass activity values that correspond to the anodic peak A0 and region A, respectively, are obtained at the PtCo_{fiber}/Cu catalyst that have a Pt loading of 5.4 μg cm⁻², compared with those at the catalysts that have Pt loadings of 15.4 μg cm⁻² and 28.7 μg cm⁻².

Comparable positive-potential going stabilized voltammograms (5 cycles) of the oxidation of N₂H₄ recorded for the Co_{fiber}/Cu and different AuCo_{fiber}/Cu catalysts are shown in Fig. 15a.

It is clearly seen that hydrazine oxidation is a potential dependent process. Furthermore, the electrochemical behavior of the AuCo_{fiber}/Cu catalysts in the N₂H₄ solution occurs in the same manner as on the PtCo_{fiber}/Cu catalysts (Fig. 14).

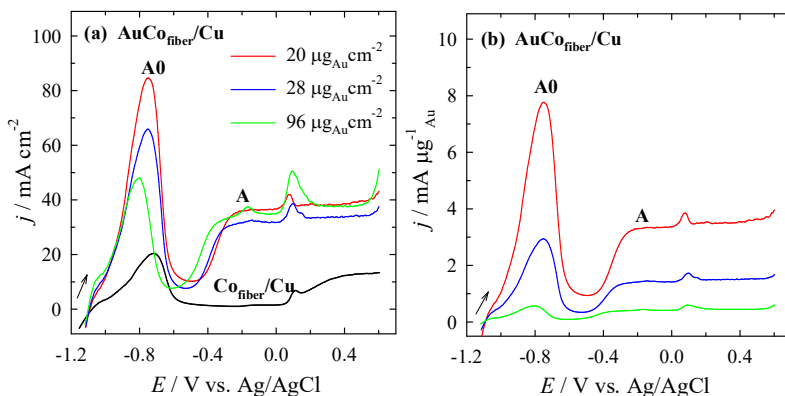


Figure 15. (a) Positive-potential going voltammograms (5 cycles) of the $\text{Co}_{\text{fiber}}/\text{Cu}$ and $\text{AuCo}_{\text{fiber}}/\text{Cu}$ catalysts that have Au loadings of 20, 28 and $96 \mu\text{g cm}^{-2}$ recorded in a $0.05 \text{ M N}_2\text{H}_4 + 1 \text{ M NaOH}$ solution at 10 mV s^{-1} ; $25 \text{ }^\circ\text{C}$. (b) The data were normalized by the Au loading for each catalyst.

In the positive-potential going voltammograms a typical current peak in the low potential region (peak A0), followed by a current plateau at higher potential values (region A), which indicates the diffusion-controlled process of the oxidation of N_2H_4 , are clearly observed (Fig. 15a). Notably, the measured current density values under peak A0 and region A are significantly higher on the $\text{AuCo}_{\text{fiber}}/\text{Cu}$ catalysts as compared with those of the pure $\text{Co}_{\text{fiber}}/\text{Cu}$ catalyst, indicating a high electrocatalytic activity of the $\text{AuCo}_{\text{fiber}}/\text{Cu}$ catalysts for the oxidation of N_2H_4 . Additionally, the measured N_2H_4 oxidation current density values that correspond to the peak A0 are ca. 4.1, 3.2 and 2.4 times greater on the $\text{AuCo}_{\text{fiber}}/\text{Cu}$ catalysts that have Au loadings of 20, 28 and $96 \mu\text{g}_{\text{Au}} \text{ cm}^{-2}$, respectively, compared with those for a pure $\text{Co}_{\text{fiber}}/\text{Cu}$ catalyst (Fig. 15a). The N_2H_4 oxidation current density values that correspond to the region A at a potential value of -0.2 V are ca. 32.7, 28.7 and 32.4 times higher on the $\text{AuCo}_{\text{fiber}}/\text{Cu}$ catalysts that have Au loadings of 20, 28 or $96 \mu\text{g}_{\text{Au}}$

cm^{-2} , respectively, compared with those for $\text{Co}_{\text{fiber}}/\text{Cu}$ (Fig. 15a). Moreover, N_2H_4 oxidation mass activity values at a potential value of -0.8 V is ca. 1.8 and 8.5 and at a potential value of -0.2 V is ca. 1.6 and 4.8 times higher on the $\text{AuCo}_{\text{fiber}}/\text{Cu}$ catalyst that have the Au loading of $20 \mu\text{g}_{\text{Au}} \text{cm}^{-2}$ as compared with those on the catalysts that have Au loadings of 28 and $96 \mu\text{g}_{\text{Au}} \text{cm}^{-2}$, respectively (Fig. 15b).

Stability of the $\text{Co}_{\text{fiber}}/\text{Cu}$, $\text{PtCo}_{\text{fiber}}/\text{Cu}$ and $\text{AuCo}_{\text{fiber}}/\text{Cu}$ catalysts has been investigated by chronoamperometry and the corresponding chronoamperograms are shown in Figs. 16 and 17.

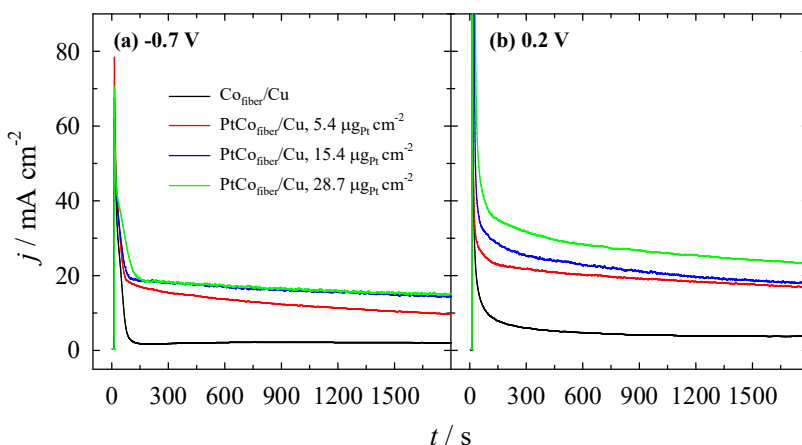


Figure 16. Chronoamperometric data for the $\text{Co}_{\text{fiber}}/\text{Cu}$ and $\text{PtCo}_{\text{fiber}}/\text{Cu}$ catalysts that have Pt loadings of 5.4, 15.4, and $28.7 \mu\text{g} \text{cm}^{-2}$ recorded in a $0.05 \text{ M N}_2\text{H}_4 + 1 \text{ M NaOH}$ solution at a constant potential value of -0.7 V (a) and 0.2 V (b), respectively, for 1800 s; at 25°C .

The chronoamperometric measurements of $\text{Co}_{\text{fiber}}/\text{Cu}$, $\text{Co}_{\text{fiber}}/\text{Cu}$ modified with Pt nanoparticles, performed at -0.7 V and 0.2 V, and $\text{Co}_{\text{fiber}}/\text{Cu}$ modified with Au nanoparticles, performed at -0.8 V and -0.2 V, confirmed the larger activity of the investigated $\text{PtCo}_{\text{fiber}}/\text{Cu}$ and $\text{AuCo}_{\text{fiber}}/\text{Cu}$ catalysts towards the oxidation of N_2H_4 , compared with that of a pure $\text{Co}_{\text{fiber}}/\text{Cu}$ (Figs. 16, 17). For all

of them, a current drop-off of the oxidation of N_2H_4 on the $\text{Co}_{\text{fiber}}/\text{Cu}$, $\text{PtCo}_{\text{fiber}}/\text{Cu}$ and $\text{AuCo}_{\text{fiber}}/\text{Cu}$ catalysts was observed, whereas, at the end of the experiment ($t = 1800$ s) all of the $\text{PtCo}_{\text{fiber}}/\text{Cu}$ and $\text{AuCo}_{\text{fiber}}/\text{Cu}$ catalysts outperformed the pure $\text{Co}_{\text{fiber}}/\text{Cu}$ catalyst.

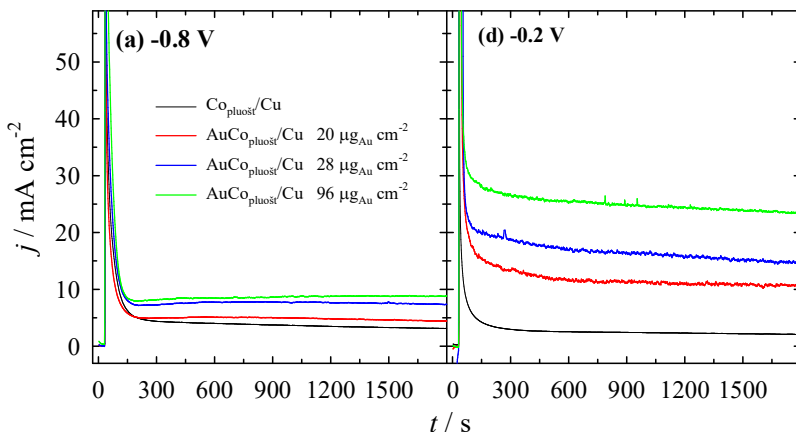


Figure 17. CA data for the $\text{Co}_{\text{fiber}}/\text{Cu}$ and $\text{AuCo}_{\text{fiber}}/\text{Cu}$ catalysts that have Au loadings of 20, 28 and $96 \mu\text{g cm}^{-2}$ recorded in a $0.05 \text{ M N}_2\text{H}_4 + 1 \text{ M NaOH}$ solution at constant potential values of -0.8 V (a) and -0.2 V (d) for 1800 s; at $25 \text{ }^\circ\text{C}$.

In the case of $\text{PtCo}_{\text{fiber}}/\text{Cu}$ catalysts, the N_2H_4 oxidation current density values measured at constant potential values of -0.7 V (Fig. 16a) and 0.2 V (Fig. 16b) are ca. 5-7 and 4.5-6, respectively, times greater than those for the pure $\text{Co}_{\text{fiber}}/\text{Cu}$ catalyst. Furthermore, the measured N_2H_4 oxidation current density values at constant potential values of -0.8 (Fig. 17a) and -0.2 V (Fig. 17b) are ca. 1.4-2.9 and 5-11, respectively, times higher at the $\text{AuCo}_{\text{fiber}}/\text{Cu}$ catalysts compared with those on the pure $\text{Co}_{\text{fiber}}/\text{Cu}$ catalyst.

3.3. Investigation of NaBH₄ hydrolysis on Co_{fiber}/Cu, AuCo_{fiber}/Cu and PtCo_{fiber}/Cu catalysts

The activity of the Co_{fiber}/Cu, AuCo_{fiber}/Cu, and PtCo_{fiber}/Cu catalysts for the hydrolysis of NaBH₄ has been investigated. Figure 18 shows the volume of generated hydrogen with respect to reaction time catalyzed by Co_{fiber}/Cu in a 5 wt.% NaBH₄ + 0.4 wt.% NaOH solution at different temperatures.

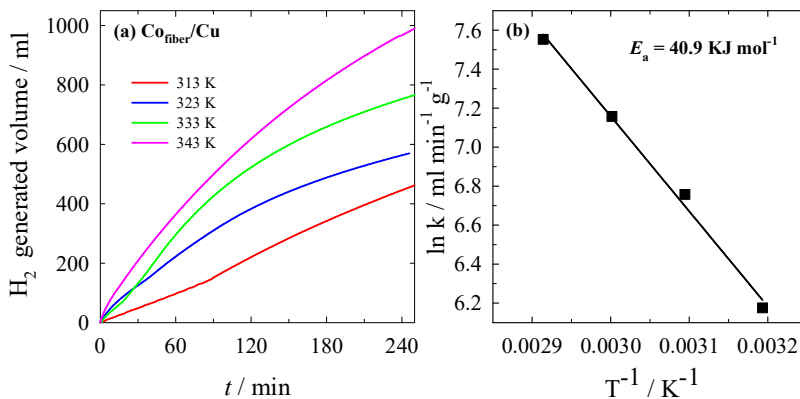


Figure 18. (a) H₂ generation from 15 ml 5 wt.% NaBH₄ + 0.4 wt.% NaOH catalyzed by Co_{fiber}/Cu at different temperatures. (b) The Arrhenius plot calculated from the rates of NaBH₄ hydrolysis in a same solution.

It has been determined that the rate of catalytic hydrolysis of NaBH₄ in an alkaline medium exponentially increased with an increase in reaction temperature, and a maximum value of 1.6 L min⁻¹ g⁻¹ was obtained at a temperature of 70 °C. The temperature dependence of the rate of H₂ generation can be expressed by the Arrhenius equation, as follows:

$$k = Ae^{-E_a/RT} \quad (3)$$

where k is the rate constant, E_a is the activation energy (J), A is the frequency factor, and R is the universal gas constant ($8.314 \text{ J mol}^{-1} \text{ K}^{-1}$). In order to find the values of E_a and A , an Arrhenius plot of $\ln(k)$ vs. $1/T$ was constructed from the data presented in Fig. 18a, and is illustrated in Fig. 18b. An activation energy of 40.9 kJ mol^{-1} for $\text{Co}_{\text{fiber}}/\text{Cu}$ was calculated from this plot.

H_2 generation rates measured for the $\text{AuCo}_{\text{fiber}}/\text{Cu}$ catalyst that have the Au loading of $28.0 \text{ } \mu\text{g cm}^{-2}$ (a) and $\text{PtCo}_{\text{fiber}}/\text{Cu}$ catalyst that have the Pt loading of $28.7 \text{ } \mu\text{g cm}^{-2}$ (c) at different temperatures are summarized in Fig. 19 and Table 4.

Table 4. H_2 generation rate obtained from 15 ml of 5 wt.% NaBH_4 + 0.4 wt.% NaOH solution catalyzed by the $\text{AuCo}_{\text{fiber}}/\text{Cu}$ and $\text{PtCo}_{\text{fiber}}/\text{Cu}$ catalysts.

T, K	$\text{AuCo}_{\text{fiber}}/\text{Cu}$ catalysts		$\text{PtCo}_{\text{fiber}}/\text{Cu}$ catalysts	
	Au loading, $\mu\text{g cm}^{-2}$	H_2 generation rate, $\text{L min}^{-1} \text{ g}^{-1}_{\text{Au}}$	Pt loading, $\mu\text{g cm}^{-2}$	H_2 generation rate, $\text{L min}^{-1} \text{ g}^{-1}_{\text{Pt}}$
303	28.0	158.8	28.7	67.5
313		265.6		154.9
323		423.5		420.6
333		719.5		630.3
343		1012.3		1238.3
323	20.0	406.0	5.4	1155.4
323	96.0	132.9	15.4	600.6

In all cases, the rate of catalytic hydrolysis of NaBH_4 in alkaline conditions exponentially increased with increasing reaction temperature. The Arrhenius plots calculated from the rates of NaBH_4 hydrolysis for these catalysts are shown in Fig. 19b and d. Based on these plots, activation energies were determined to be 40.7 kJ mol^{-1} for $\text{AuCo}_{\text{fiber}}/\text{Cu}$ and 62.6 kJ mol^{-1} for $\text{PtCo}_{\text{fiber}}/\text{Cu}$.

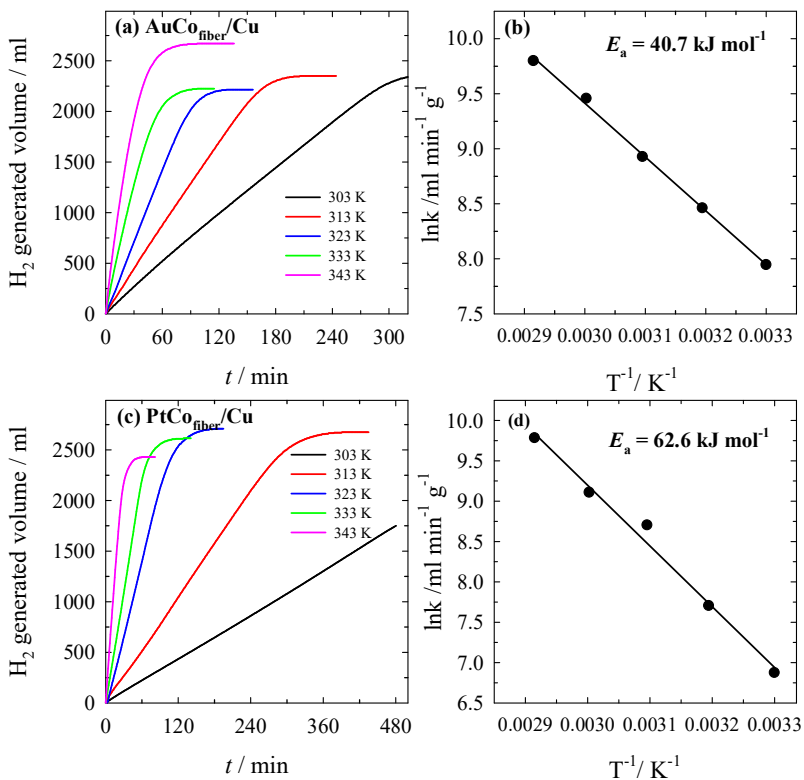


Figure 19. H₂ generation from 15 ml 5 wt.% NaBH₄ + 0.4 wt.% NaOH catalyzed by the AuCo_{fiber}/Cu catalyst that have the Au loading of 28.0 μg cm⁻² (a) and the PtCo_{fiber}/Cu catalyst that have the Pt loading of 28.7 μg cm⁻² (c) at different temperatures. (b, d) The Arrhenius plot calculated from the rates of NaBH₄ hydrolysis in a same solution.

The H₂ generation rate obtained for PtCo_{fiber}/Cu (28.7 μg cm⁻²) at a temperature of 70 °C was higher than that at AuCo_{fiber}/Cu (28 μg cm⁻²) and totaled 1238.3 L min⁻¹ g⁻¹_{Pt} and 1012.3 L min⁻¹ g⁻¹_{Au}, respectively.

Figure 20 shows the rates of H₂ generation from NaBH₄ solution when catalyzed by the investigated AuCo_{fiber}/Cu and PtCo_{fiber}/Cu catalysts at a temperature of 50 °C.

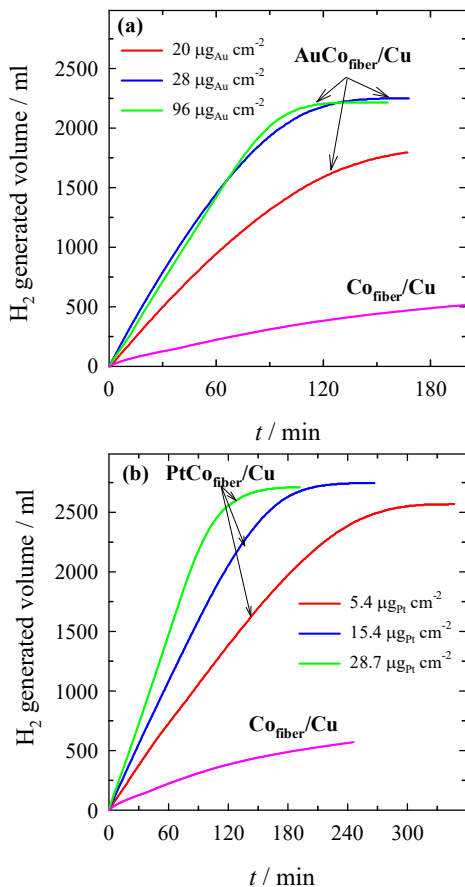


Figure 20. H₂ generation from 15 ml 5 wt.% NaBH₄ + 0.4 wt.% NaOH at 50 °C catalyzed by the Co_{fiber}/Cu, AuCo_{fiber}/Cu and PtCo_{fiber}/Cu catalysts that have different Au and Pt loadings.

Significantly higher H₂ generation rates were obtained with the AuCo_{fiber}/Cu and PtCo_{fiber}/Cu catalysts (Table 4) as compared to those with Co_{fiber}/Cu (1.6 L min⁻¹ g⁻¹). Notably, the H₂ generation rate also depends on the amount of Au or Pt loadings on the prepared catalysts. Comparing the performance of the AuCo_{fiber}/Cu catalysts in terms of the amount of Au loadings (ranging between 20-96 μg cm⁻²) at a temperature of 50 °C, the maximum H₂ generation rate of 423.5 L min⁻¹ g⁻¹_{Au} was obtained at an Au loading of 28.0 μg cm⁻². In the case of the PtCo_{fiber}/Cu catalysts that have Pt loadings in the range of 5-29 μg cm⁻², the highest H₂ generation rate of 1155.4 L min⁻¹ g⁻¹_{Pt} at a temperature of 50 °C was obtained at the lowest amount of Pt loading (5.4 μg cm⁻²). Therefore, these results confirm that the fiber-shaped Co coatings decorated with Au or Pt crystallites efficiently catalyzed the hydrolysis of NaBH₄ in alkaline conditions.

3.4. NaBH₄-H₂O₂ and N₂H₄-H₂O₂ fuel cell test experiments

The stability of the Au nanoparticles modified fiber-shaped Co catalysts deposited on the Cu surface has been examined in DBHPFC and DHHPFC single fuel cells. An alkaline direct NaBH₄-H₂O₂ and N₂H₄-H₂O₂ fuel cells were constructed with the Co_{fiber}/Cu and different AuCo_{fiber}/Cu catalysts that have Au loadings of 10.9, 22.4 and 84.4 μg cm⁻² as the anode and Pt sheet as the cathode. The solutions of 1 M NaBH₄ or 1 M N₂H₄ in 4 M NaOH and 5 M H₂O₂ in 1.5 M HCl were used as the anolyte and catholyte, respectively. The obtained fuel cell polarization curves and the corresponding power density curves against the current density by employing the prepared Co_{fiber}/Cu and AuCo_{fiber}/Cu catalysts as the anodes for DBHPFC and DHHPFC are presented in Fig. 21. The main obtained parameters are summarized in Table 5. The direct N₂H₄-H₂O₂ and NaBH₄-H₂O₂ fuel cells exhibited an open circuit voltage of ca. 1.7 and 1.9 V, respectively. It was found that in both types of fuel cells power density values are higher in the case of the investigated AuCo_{fiber}/Cu

catalysts as compared to those of $\text{Co}_{\text{fiber}}/\text{Cu}$ (Fig. 21). The deposition of low amounts of Au nanoparticles on the fiber-shaped Co coating resulted in an enhanced peak power densities for direct $\text{N}_2\text{H}_4\text{-H}_2\text{O}_2$ and $\text{NaBH}_4\text{-H}_2\text{O}_2$ fuel cells as compared to those of pure $\text{Co}_{\text{fiber}}/\text{Cu}$.

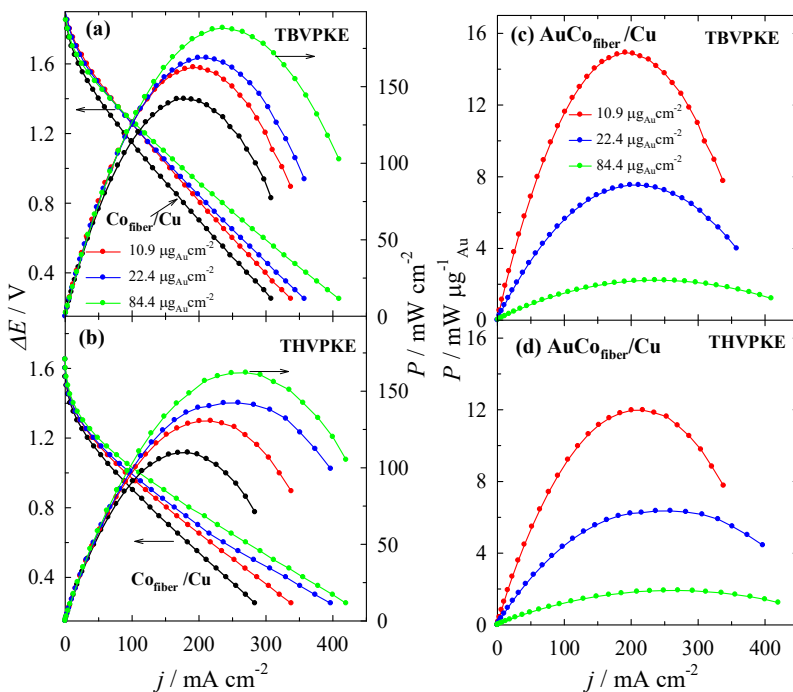


Figure 21. Cell polarization and power density curves for the DBHPFC (a) and DHHPFC (b) using $\text{Co}_{\text{fiber}}/\text{Cu}$ and $\text{AuCo}_{\text{fiber}}/\text{Cu}$ anode catalysts with anolyte consisted of 1 M NaBH_4 + 4 M NaOH or 1 M N_2H_4 + 4 M NaOH and 5 M H_2O_2 + 1.5 M HCl catholyte at 25 °C. Specific power density values normalized by the Au loadings for each catalysts in DBHPFC (c) and DHHPFC (d).

Table 5. Electrochemical parameters of DHHPFC and DBHPFC employing the $\text{Co}_{\text{fiber}}/\text{Cu}$, $\text{AuCo}_{\text{fiber}}/\text{Cu}$ and $\text{PtCo}_{\text{fiber}}/\text{Cu}$ catalysts as the anode.

KE	Anode, loading, $\mu\text{g cm}^{-2}$	E_{cell} , V	j , mA cm^{-2}	P, mW cm^{-2}	P, $\text{mW } \mu\text{g}^{-1}_{\text{Au or Pt}}$	P, $\text{mW mg}^{-1}_{\text{cat}}$
DBHPFC	$\text{Co}_{\text{fiber}}/\text{Cu}$, 2353	0.80	177.0	142.0	–	60.3
	$\text{AuCo}_{\text{fiber}}/\text{Cu}$, 10.9	0.85	191.0	163.0	14.9	100.2
	$\text{AuCo}_{\text{fiber}}/\text{Cu}$, 22.4	0.80	211.0	169.0	7.5	107.5
	$\text{AuCo}_{\text{fiber}}/\text{Cu}$, 84.4	0.80	235.0	188.0	2.2	173.0
DHHPFC	$\text{Co}_{\text{fiber}}/\text{Cu}$, 2353	0.60	183.0	110.0	–	46.7
	$\text{AuCo}_{\text{fiber}}/\text{Cu}$, 10.9	0.60	218.0	131.0	12.0	80.5
	$\text{AuCo}_{\text{fiber}}/\text{Cu}$, 22.4	0.55	259.0	142.0	6.3	90.3
	$\text{AuCo}_{\text{fiber}}/\text{Cu}$, 84.4	0.60	270.0	162	1.9	149.3
DHHPFC	$\text{Co}_{\text{fiber}}/\text{Cu}$, 2353	0.60	183.1	109.9	–	46.7
	$\text{PtCo}_{\text{fiber}}/\text{Cu}$, 5.4	0.60	197.2	118.4	21.9	50.2
	$\text{PtCo}_{\text{fiber}}/\text{Cu}$, 15.4	0.65	200.2	130.2	8.4	55.0
	$\text{PtCo}_{\text{fiber}}/\text{Cu}$, 28.7	0.65	229.7	149.4	5.2	62.7

Moreover, highest peak power density values up to 162 mW cm^{-2} for DHHPFC and 188 mW cm^{-2} for DBHPFC were obtained at a temperature of 25°C using the $\text{AuCo}_{\text{fiber}}/\text{Cu}$ catalyst that have the Au loading of $84.4 \mu\text{g cm}^{-2}$ as the anode. In order to compare the power density of the prepared $\text{AuCo}_{\text{fiber}}/\text{Cu}$ catalysts, the obtained values were normalized by the Au loading for each catalyst. The summarized data are given in Fig. 21c, d and Table 5. It should be noted that highest specific peak power density values of $12.0 \text{ mW } \mu\text{g}^{-1}_{\text{Au}}$ for $\text{N}_2\text{H}_4\text{-H}_2\text{O}_2$ and $14.9 \text{ mW } \mu\text{g}^{-1}_{\text{Au}}$ for $\text{NaBH}_4\text{-H}_2\text{O}_2$ were obtained, when employing the $\text{AuCo}_{\text{fiber}}/\text{Cu}$ catalyst that have the lowest Au loading of $10.9 \mu\text{g cm}^{-2}$ as the anode material.

Therefore, a fiber-shaped Co coating and that modified with low amounts of Au nanoparticles would be promising anode catalysts for the application of direct $\text{N}_2\text{H}_4\text{-H}_2\text{O}_2$ and $\text{NaBH}_4\text{-H}_2\text{O}_2$ fuel cells.

Figure 22 presents the obtained fuel cell polarization curves and the corresponding power density curves against the current density by employing the prepared $\text{Co}_{\text{fiber}}/\text{Cu}$ and $\text{PtCo}_{\text{fiber}}/\text{Cu}$ catalysts as the anodes for DHHPFC. The direct $\text{N}_2\text{H}_4\text{-H}_2\text{O}_2$ fuel cell exhibited an open circuit voltage of ca. 1.7. Moreover, the power density values are higher in the case of the investigated $\text{PtCo}_{\text{fiber}}/\text{Cu}$ catalysts as compared to those of $\text{Co}_{\text{fiber}}/\text{Cu}$ (Fig. 22). Highest peak power density up to 149 mW cm^{-2} for DHHPFC was obtained at a temperature of 25°C using the $\text{PtCo}_{\text{fiber}}/\text{Cu}$ catalyst that have the Pt loading of $28.7 \mu\text{g cm}^{-2}$ as the anode.

To compare the power density of the prepared $\text{PtCo}_{\text{fiber}}/\text{Cu}$ catalysts, the obtained power density values were normalized by the Pt loadings for each catalyst. The summarized data are given in Fig. 22b and Table 5. As seen, the highest specific peak power density value of $21.9 \text{ mW } \mu\text{g}^{-1}_{\text{Pt}}$ for $\text{N}_2\text{H}_4\text{-H}_2\text{O}_2$ was obtained, when employing the $\text{PtCo}_{\text{fiber}}/\text{Cu}$ catalyst that have the lowest Pt loading of $5.4 \mu\text{g cm}^{-2}$ as the anode material (Table 5). It is evident that the prepared $\text{PtCo}_{\text{fiber}}/\text{Cu}$ catalysts are promising materials and can be used as anode catalysts in direct $\text{N}_2\text{H}_4\text{-H}_2\text{O}_2$ fuel cells.

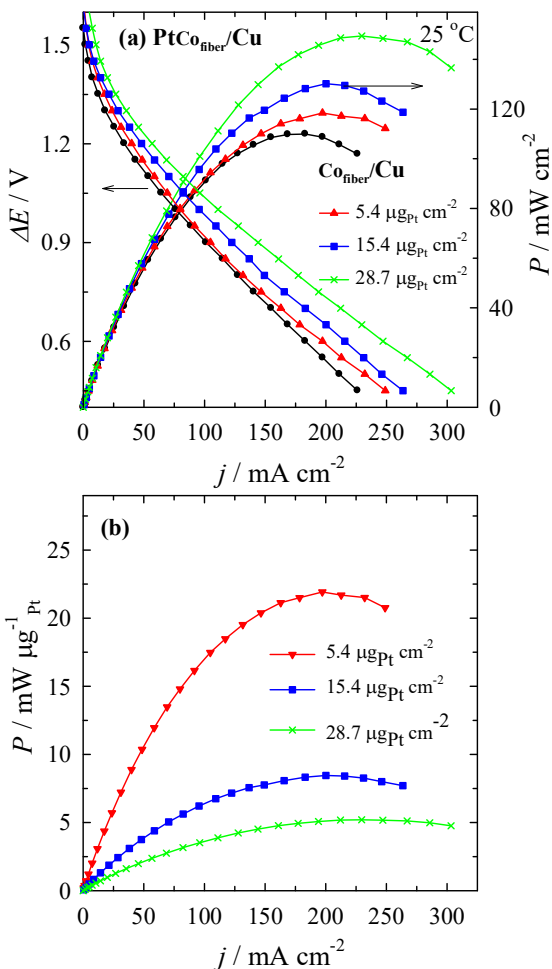


Figure 22. (a) Cell polarization and power density curves for the DHHPFC using the $\text{Co}_{\text{fiber}}/\text{Cu}$ and $\text{PtCo}_{\text{fiber}}/\text{Cu}$ anode catalysts with anolyte consisted of $1 \text{ M N}_2\text{H}_4 + 4 \text{ M NaOH}$ and $5 \text{ M H}_2\text{O}_2 + 1.5 \text{ M HCl}$ catholyte at 25°C . (b) Specific power density values normalized by the Pt loading for each catalyst.

CONCLUSIONS

1. It has been found that Au nanoparticles modified ZnCo/Ti catalysts that have the Au loading in the range from 31 up to 306 $\mu\text{g cm}^{-2}$ exhibit significantly higher electrocatalytic activity for the oxidation reactions of sodium borohydride and hydrazine as compared with that of ZnCo/Ti. The sodium borohydride and hydrazine oxidation current density values measured on the AuZnCo/Ti catalyst with a different Au loading are about 2 times higher than those obtained on ZnCo/Ti.
2. The PtCo_{fiber}/Cu and AuCo_{fiber}/Cu catalysts have been prepared with Pt and Au loadings in the range from 5.4 up to 28.7 $\mu\text{g cm}^{-2}$ and from 20 up to 96 $\mu\text{g cm}^{-2}$, respectively, also exhibit significantly higher electrocatalytic activity for the oxidation of sodium borohydride and hydrazine as well as for the hydrolysis of sodium borohydride as compared with that of Co_{fiber}/Cu. Hydrazine oxidation current density values measured on the AuCo_{fiber}/Cu and PtCo_{fiber}/Cu catalysts are approximately 32 and 6, respectively, times higher than those on the pure Co_{fiber}/Cu catalyst, whereas, the sodium borohydride current density values measured on the same catalysts are about 2 and 4-6 times higher in comparison with those for pure Co_{fiber}/Cu.
3. The AuCo_{fiber}/Cu and PtCo_{fiber}/Cu catalysts exhibit significantly higher catalytic activity for the hydrolysis of sodium borohydride as compared with that obtained for Co_{fiber}/Cu. It has been determined that highest hydrogen generation rates of 1012.3 L min⁻¹ g⁻¹_{Au} and 1238.3 L min⁻¹ g⁻¹_{Pt} have been obtained for the AuCo_{fiber}/Cu and PtCo_{fiber}/Cu catalysts, respectively, at a temperature of 70 °C, corresponding to Au and Pt loadings of 20 $\mu\text{g cm}^{-2}$ and 28.7 $\mu\text{g cm}^{-2}$.

4. The activity and stability of the $\text{AuCo}_{\text{fiber}}/\text{Cu}$ and $\text{PtCo}_{\text{fiber}}/\text{Cu}$ catalysts have been investigated by applying them as the anode material in $\text{NaBH}_4\text{-H}_2\text{O}_2$ and $\text{N}_2\text{H}_4\text{-H}_2\text{O}_2$ fuel cell prototypes at a temperature of $25\text{ }^\circ\text{C}$. It has been found that the maximum power density of the $\text{NaBH}_4\text{-H}_2\text{O}_2$ and $\text{N}_2\text{H}_4\text{-H}_2\text{O}_2$ fuel cell prototypes at a temperature of $25\text{ }^\circ\text{C}$ is 188 mW cm^{-2} and 162 mW cm^{-2} , respectively, using the $\text{AuCo}_{\text{fiber}}/\text{Cu}$ catalyst that have the Au loading of $84.4\text{ }\mu\text{g cm}^{-2}$ as the anode, whereas highest specific peak power density values of $14.9\text{ mW }\mu\text{g}^{-1}_{\text{Au}}$ and $12.0\text{ mW }\mu\text{g}^{-1}_{\text{Au}}$ have been obtained, when employing the $\text{AuCo}_{\text{fiber}}/\text{Cu}$ catalyst that have the Au loading of $10.9\text{ }\mu\text{g cm}^{-2}$ as the anode in $\text{NaBH}_4\text{-H}_2\text{O}_2$ and $\text{N}_2\text{H}_4\text{-H}_2\text{O}_2$, respectively, fuel cell prototypes. Using the $\text{PtCo}_{\text{fiber}}/\text{Cu}$ anode catalyst that have the Pt loading of $28.7\text{ }\mu\text{g cm}^{-2}$ in the $\text{N}_2\text{H}_4\text{-H}_2\text{O}_2$ fuel cell prototype, the highest peak power density is 149 mW cm^{-2} at a temperature of $25\text{ }^\circ\text{C}$. Moreover, the greatest specific peak power density value of $21.9\text{ mW }\mu\text{g}^{-1}_{\text{Pt}}$ has been obtained, when employing the catalyst that have the Pt loading of $5.4\text{ }\mu\text{g cm}^{-2}$ as the anode material.
5. Based on testing experiments of $\text{NaBH}_4\text{-H}_2\text{O}_2$ and $\text{N}_2\text{H}_4\text{-H}_2\text{O}_2$ fuel cell prototypes, it is evident that the prepared $\text{AuCo}_{\text{fiber}}/\text{Cu}$ and $\text{PtCo}_{\text{fiber}}/\text{Cu}$ catalysts are promising materials and can be used as anode catalysts in direct $\text{NaBH}_4\text{-H}_2\text{O}_2$ and $\text{N}_2\text{H}_4\text{-H}_2\text{O}_2$ fuel cells

SUMMARY IN LITHUANIAN

Šiame darbe buvo kuriamos naujos efektyvios medžiagos, panaudojant netauriųjų metalų cinko-kobalto (ZnCo) ir kobalto, turinčio pluoštelinę struktūrą ($\text{Co}_{\text{pluošt}}$), dangas bei jas toliau modifikuojant nedideliais Au ar Pt nanodalelių kiekiais, siekiant pakeisti gerai žinomus ir brangius Pt ir Au ar jų lydinių katalizatorius, naudojamus kaip anodo medžiagas įvairiuose kuro elementuose. Disertacinio darbo metu buvo formuojami ZnCo/Ti, AuZnCo/Ti, $\text{Co}_{\text{pluošt}}/\text{Ti}(\text{Cu})$, $\text{AuCo}_{\text{pluošt}}/\text{Cu}$ ir $\text{PtCo}_{\text{pluošt}}/\text{Cu}$ katalizatoriai, taikant elektrocheminį metalų nusodinimo ir galvaninio pakeitimo metodus. Ištirtos ir optimizuotos pastarųjų katalizatorių gavimo sąlygos, o jų aktyvumas buvo įvertintas NaBH_4 ir N_2H_4 oksidacijos bei NaBH_4 hidrolizės reakcijoms. Taip pat $\text{Co}_{\text{pluošt}}/\text{Cu}$, $\text{AuCo}_{\text{pluošt}}/\text{Cu}$ ir $\text{PtCo}_{\text{pluošt}}/\text{Cu}$ katalizatorių aktyvumas bei stabilumas buvo tiriamas, juos panaudojant anodo medžiagomis $\text{NaBH}_4\text{-H}_2\text{O}_2$ ir $\text{N}_2\text{H}_4\text{-H}_2\text{O}_2$ kuro elementų prototipuose.

Nustatyta, kad Au nanodalelėmis modifikuoti ZnCo/Ti katalizatoriai, kuriuose nusodinto Au įkrova yra nuo 31 iki 306 $\mu\text{g cm}^{-2}$, pasižymi ženkliai didesniu elektrokataliziniu aktyvumu NaBH_4 ir N_2H_4 oksidacijos reakcijoms nei ZnCo/Ti katalizatorius. Sukurti $\text{PtCo}_{\text{pluošt}}/\text{Cu}$ ir $\text{AuCo}_{\text{pluošt}}/\text{Cu}$ katalizatoriai, kuriuose Pt ir Au įkrovos yra atitinkamai nuo 5,4 iki 28,7 $\mu\text{g}_{\text{Pt}} \text{cm}^{-2}$ ir nuo 20 iki 96 $\mu\text{g}_{\text{Au}} \text{cm}^{-2}$ taip pat pasižymi itin dideliu aktyvumu NaBH_4 ir N_2H_4 oksidacijos reakcijoms bei NaBH_4 hidrolizės reakcijai, palyginus su gryno $\text{Co}_{\text{pluošt}}/\text{Cu}$ katalizatoriaus aktyvumu. Be to, išmatuoti didžiausi $\text{NaBH}_4\text{-H}_2\text{O}_2$ ir $\text{N}_2\text{H}_4\text{-H}_2\text{O}_2$ kuro elementų prototipų galios tankiai, esant 25 °C temperatūrai, yra, atitinkamai, 188 mW cm^{-2} ir 162 mW cm^{-2} , panaudojant $\text{AuCo}_{\text{pluošt}}/\text{Cu}$ katalizatorių su nusodinto Au įkrova 84,4 $\mu\text{g cm}^{-2}$ kaip anodą. Naudojant $\text{PtCo}_{\text{pluošt}}/\text{Cu}$ katalizatorių su nusodintos Pt įkrova 5,4 $\mu\text{g cm}^{-2}$ anodu $\text{N}_2\text{H}_4\text{-H}_2\text{O}_2$ kuro elemento prototipe, išmatuotas didžiausias galios tankis yra 149 mW cm^{-2} , esant 25 °C temperatūrai. Remiantis atliktais katalizatorių testavimo

eksperimentais laboratoriniuose $\text{NaBH}_4\text{-H}_2\text{O}_2$ ir $\text{N}_2\text{H}_4\text{-H}_2\text{O}_2$ kuro elementų prototipuose, matyti, kad suformuoti $\text{AuCo}_{\text{pluošt}}/\text{Cu}$ ir $\text{PtCo}_{\text{pluošt}}/\text{Cu}$ katalizatoriai yra perspektyvios medžiagos ir gali būti naudojamos anodo katalizatoriais tiesioginiuose $\text{NaBH}_4\text{-H}_2\text{O}_2$ ir $\text{N}_2\text{H}_4\text{-H}_2\text{O}_2$ kuro elementuose.

LIST OF PUBLICATIONS

In Clarivate Analytics Web of Science

1. L. Tamašauskaitė-Tamašiūnaitė, S. Lichušina, A. Balčiūnaitė, A. Zabelaitė, D. Šimkūnaitė, J. Vaičiūnienė, I. Stalnionienė, A. Žielienė, A. Selskis, E. Norkus “*Zinc-cobalt alloy deposited on the titanium surface as electrocatalysts for borohydride oxidation*“. J. Electrochem. Soc. 162 (2015) F348-F353.
2. A. Balčiūnaitė, A. Zabelaitė, L. Tamašauskaitė-Tamašiūnaitė, E. Norkus. “*Employment of fiber-shaped Co modified with Au nanoparticles as anode in direct $\text{NaBH}_4\text{-H}_2\text{O}_2$ and $\text{N}_2\text{H}_4\text{-H}_2\text{O}_2$ fuel cells*”. J. Electrochem. Soc. 165(14) (2018) F1249-F1253.
3. A. Zabelaitė, A. Balčiūnaitė, I. Stalnionienė, S. Lichušina, D. Šimkūnaitė, J. Vaičiūnienė, B. Šimkūnaitė-Stanyrienė, A. Selskis, L. Tamašauskaitė-Tamašiūnaitė, E. Norkus. “*Fiber-shaped Co modified with Au and Pt crystallites for enhanced hydrogen generation from sodium borohydride*”. Int. J. Hydrogen Energy 43 (2018) 23310-23318.
4. A. Zabelaitė, A. Balčiūnaitė, D. Šimkūnaitė, J. Vaičiūnienė, A. Selskis, L. Naruškevičius, L. Tamašauskaitė-Tamašiūnaitė, E. Norkus. “*Investigation of borohydride and hydrazine electro-oxidation on gold nanoparticles modified zinc-cobalt coating*”. Chemija 30(3) (2019) (accepted for publication).
5. A. Zabelaitė, A. Balčiūnaitė, D. Šimkūnaitė, S. Lichušina, I. Stalnionienė, B. Šimkūnaitė-Stanyrienė, L. Naruškevičius, L. Tamašauskaitė-Tamašiūnaitė, E. Norkus. “*Fiber-like cobalt decorated with platinum crystallites as electrocatalysts for hydrazine electro-oxidation*“. J. Electrochem. Soc. (2019) (submitted for press).
6. A. Zabelaitė, D. Šimkūnaitė, A. Balčiūnaitė, B. Šimkūnaitė-Stanyrienė, I. Stalnionienė, L. Naruškevičius, A. Selskis, L. Tamašauskaitė-Tamašiūnaitė, E. Norkus. “*ZnCo alloy modified*

with Au nanoparticles as electrocatalyst for borohydride electro-oxidation". J. Electrochem. Soc. (2019) (submitted for press).

In Other Referred International Journals

1. L. Tamašauskaitė-Tamašiūnaitė, S. Lichušina, D. Šimkūnaitė, A. Zabielaite, D. Šimkūnaitė, J. Vaičiūnienė, A. Selskis, E. Norkus. "*Zinc-cobalt alloy deposited on the titanium surface as electrocatalysts for borohydride oxidation*". ECS Transactions 61(29) (2014) 49-58.
2. A. Balčiūnaitė, S. Lichušina, D. Šimkūnaitė, A. Zabielaite, A. Selskis, L. Tamašauskaitė-Tamašiūnaitė, E. Norkus. "*Gold-zinc-cobalt deposited on titanium as electrocatalysts for borohydride oxidation*". ECS Transactions 64(3) (2014) 1103-1112.
3. A. Balčiūnaitė, A. Zabielaite, L. Tamašauskaitė-Tamašiūnaitė, E. Norkus. "*Employment of fiber-shaped cobalt modified with gold nanoparticles as anode in direct borohydride and hydrazine fuel cells*". ECS Transactions 85(13) (2018) 935-941.

Publications in International Conferences

1. L. Tamašauskaitė-Tamašiūnaitė, S. Lichušina, A. Balčiūnaitė, A. Zabielaite, D. Šimkūnaitė, J. Vaičiūnienė, A. Selskis, E. Norkus. "*Zinc-cobalt alloy deposited on the titanium surface as electrocatalysts for borohydride oxidation*". 225th ECS Meeting: Orlando, USA (2014) E5-596.
2. A. Balčiūnaitė, S. Lichušina, D. Šimkūnaitė, A. Zabielaite, A. Selskis, L. Tamašauskaitė-Tamašiūnaitė, E. Norkus. "*Gold-zinc-cobalt deposited on titanium as electrocatalysts for borohydride oxidation*". 226th ECS and SMEQ Joint International Meeting: Cancun, Mexico (2014) F3-1173.
3. L. Tamašauskaitė-Tamašiūnaitė, S. Lichušina, A. Balčiūnaitė, D. Šimkūnaitė, A. Zabielaite, A. Selskis, R. Juškėnas, E. Norkus. "*Comparison of borohydride oxidation on the gold crystallites*".

- deposited on the smooth and fiber cobalt coatings*". 226th ECS and SMEQ Joint International Meeting: Cancun, Mexico (2014) F3-1176.
4. A. Zabielaitytė, L. Tamašauskaitė-Tamašiūnaitė, A. Balčiūnaitė, S. Lichušina, I. Stalnionienė, A. Jagminienė, A. Žielienė, E. Norkus. "*Decoration of fiber structure cobalt with gold nanoparticles for application in fuel cells*". 249th ACS National Meeting & Exposition: Denver, USA (2015) ENFL-288.
 5. L. Tamašauskaitė-Tamašiūnaitė, A. Zabielaitytė, S. Lichušina, A. Balčiūnaitė, I. Stalnionienė, Z. Sukackienė, D. Šimkūnaitė, A. Selskis, E. Norkus. "*Fabrication of fiber structure Co decorated with Pt nanoparticles for application in fuel cells*". 13th International Fischer symposium: Lubeck, Germany (2015) P32.
 6. L. Tamašauskaitė-Tamašiūnaitė, A. Zabielaitytė, S. Lichušina, A. Matusevičiūtė, D. Šimkūnaitė, A. Selskis, E. Norkus. "*Investigation of hydrazine oxidation at Co fiber structure decorated with Pt nanoparticles*". 66th Annual Meeting of the International Society of Electrochemistry: Taipei, Taiwan (2015) isel51825 (žodinis pranešimas).
 7. A. Zabielaitytė, L. Tamašauskaitė-Tamašiūnaitė, I. Stalnionienė, S. Lichušina, D. Šimkūnaitė, A. Matusevičiūtė, B. Šimkūnaitė-Stanygienė, A. Selskis, E. Norkus. "*Hydrogen generation from sodium borohydride catalyzed by cobalt with a fiber structure decorated with platinum nanoparticles*". 3rd ENEFM2015, International Congress on Energy Efficiency and Energy Related Materials: Oludeniz, Turkey (2015) ID 5.
 8. E. Norkus, A. Zabielaitytė, I. Stalnionienė, S. Lichušina, D. Šimkūnaitė, B. Šimkūnaitė-Stanygienė, A. Matusevičiūtė, A. Selskis, L. Tamašauskaitė-Tamašiūnaitė. "*Kinetics of sodium borohydride hydrolysis catalyzed by cobalt with a fiber structure decorated with gold or platinum nanoparticles*". The International Chemical Congress of Pacific Basin Societies

- (PACIFICHEM 2015): Honolulu, Hawaii, USA (2015) MTL5 2206.
9. A. Zabielaite, A. Balciunaitė, S. Lichušina, D. Šimkūnaitė, L. Tamašauskaitė-Tamašiūnaitė, E. Norkus. “*Investigation of hydrazine oxidation on ZnCo modified with gold nanoparticles*”. Intern. Conf. of Lith. Chem. Soc. "Chemistry and Chemical Technology 2015", dedicated to Prof. V. Daukšas 80 Birth Anniversary, Vilnius, Lithuania, Jan. 23, 2015, Programme and Proceedings of the Intern. Conf., p. 281-283.
 10. A. Zabielaite, K. Antanavičiūtė, A. Balciunaitė, L. Tamašauskaitė-Tamašiūnaitė, E. Norkus. “*Decoration of fiber structure Co with Pt or Au nanoparticles for catalytic purposes*”. 229th ECS Meeting: San Diego, USA (2016) E02-1120.
 11. L. Tamašauskaitė-Tamašiūnaitė, A. Zabielaite, K. Antanavičiūtė, A. Balciunaitė, E. Norkus. “*Decoration of cobalt with a fiber structure with gold nanoparticles for hydrazine oxidation*”. 14th International Conference on Electrified Interfaces (ICEI 2016): Singapore (2016) P 11, p. 93.
 12. L. Tamašauskaitė-Tamašiūnaitė, A. Zabielaite, I. Stalnionienė, S. Lichušina, A. Selskis, E. Norkus. “*Hydrogen generation via sodium borohydride hydrolysis using gold nanoparticles modified fiber cobalt coating deposited on titanium*”. International Conference on Pure and Applied Chemistry, ICPAC 2016: Mauritius (2016) P. 16, p. 148.
 13. A. Zabielaite, S. Lichušina, D. Šimkūnaitė, A. Selskis, L. Tamašauskaitė-Tamašiūnaitė, E. Norkus. “*Fiber cobalt decorated with platinum nanoparticles as electrocatalysts for hydrazine oxidation*”. International conference of Lithuanian Society of Chemistry “Chemistry & Chemical Technology 2016”: Vilnius, Lithuania (2016) p. 100.
 14. L. Tamašauskaitė-Tamašiūnaitė, D. Upskuvienė, A. Zabielaite, K. Antanavičiūtė, J. Vaičiūnienė, E. Norkus. “*Gold nanoparticles decorated cobalt with smooth and fiber structures*

- as electrocatalysts for glucose oxidation*". 2nd International Conference on Chemical and Biochemical Engineering (ICCB2): Canary Islands, Spain (2017) 1042.
15. A. Zabielaitytė, L. Tamašauskaitė-Tamašiūnaitė, I. Stalnionienė, S. Lichušina, D. Šimkūnaitė, E. Norkus. "*Investigation of borohydride and hydrazine oxidation on fiberlike cobalt coating decorated with platinum nanoparticles*". 19th International Conference-School Advanced Materials and Technologies: Palanga, Lithuania (2017) P100.
 16. A. Zabielaitytė, L. Tamašauskaitė-Tamašiūnaitė, A. Balčiūnaitė, I. Stankevičienė, E. Norkus. "*Non-noble metal catalysts for borohydride and hydrazine oxidation*". 4th International Conference on Computational and Experimental Science and Engineering (ICCESEN 2017) 82.
 17. L. Tamašauskaitė-Tamašiūnaitė, A. Balčiūnaitė, A. Zabielaitytė, I. Stalnionienė, S. Lichušina, V. Pakštas, E. Norkus. "*Hydrogen generation from sodium borohydride using cobalt modified with Au and Pt nanoparticles*". 7th Annual World Congress of Nano Science & Technology-2017 (Nano S&T-2017), Fukuoka, Japan (žodinis pranešimas).
 18. A. Balčiūnaitė, A. Zabielaitytė, L. Tamašauskaitė-Tamašiūnaitė, E. Norkus. "*Employment of fiber-shaped cobalt modified with gold nanoparticles as anode in direct borohydride and hydrazine fuel cells*". 233th ECS Meeting: Seattle, WA, USA (2018) ID 107884 (žodinis pranešimas).
 19. A. Balčiūnaitė, A. Zabielaitytė, L. Tamašauskaitė-Tamašiūnaitė, E. Norkus. "*Employment of AuCo catalyst as anode in direct borohydride-hydroxide peroxide fuel cells*". 8th International Advances in Applied Physics Materials Science Congress and Exhibition (APMAS2018): Oludeniz, Turkey (2018) ID 757 (žodinis pranešimas).
 20. A. Zabielaitytė, D. Upskuvienė, B. Šimkūnaitė-Stanygienė, L. Tamašauskaitė-Tamašiūnaitė, E. Norkus. "*Gold nanoparticles*

- decorated cobalt with smooth and fiber-shaped structures as electrocatalysts for glucose oxidation*". 256th ACS National Meeting Exposition: Boston, MA, USA (2018) ENFL-219.
21. D. Šimkūnaitė, A. Zabielaity, A. Balčiūnaitė, B. Šimkūnaitė-Stanyrienė, A. Selskis, L. Tamašauskaitė-Tamašiūnaitė, E. Norkus. "*Au nanoparticles decorated ZnCo alloy as a catalyst for borohydride oxidation*". 20th International Conference-School "Advanced Materials and Technologies 2018: Palanga, Lithuania (2018) P126.
 22. A. Zabielaity, L. Tamašauskaitė-Tamašiūnaitė, E. Norkus. "*Evaluation of activity of Pt nanoparticles decorated fiber-shaped Co for methanol electro-oxidation*". 9th Annual Meeting of the International Society of Electrochemistry: Bologna, Italy (2018) ID ise182891, S10-086.
 23. A. Balčiūnaitė, A. Zabielaity, Z. Sukackienė, L. Tamašauskaitė-Tamašiūnaitė, E. Norkus. "*Smooth and fiber-shaped Co coatings decorated with Pt crystallites as the anode catalysts for direct borohydride-hydrogen peroxide fuel cells*". ECS and SMEQ Joint International Meeting (AiMES 2018): Cancun, Mexico (2018) ID 114802, I01-1585 (žodinis pranešimas).
 24. E. Norkus, A. Zabielaity, D. Šimkūnaitė, J. Vaičiūnienė, V. Pakštas, L. Tamašauskaitė-Tamašiūnaitė. "*Application of platinum nanoparticles decorated fiber-shaped cobalt for methanol and ethanol oxidation*". 235th ECS Meeting: 26-31 May, Dallas, TX, USA (2019) ID IO2-1558.

CURRICULUM VITAE

Personal information

Name, surname Aušrinė Zabielaite (Vaičiukevičienė)

Address Tuskulėnų str. 7-35, Vilnius

Telephone +370 67836371

E-mail ausrine.zabielaite@ftmc.lt

Nationality Lithuanian

Date of birth 1967-03-29

Education

2007/09/01 – 2012/06/27 Bachelor degree of Education Science and Technological Education, Lithuanian University of Educational Sciences

2012/09/01 – 2014/06/27 Master degree of Education Science and Technological Education, Lithuanian University of Educational Sciences

2014-2018 PhD studies at the Department of Catalysis, Center for Physical Sciences and Technology

Work experience

2017 till now Junior Research Associate, Department of Catalysis, Center for Physical Sciences and Technology

2012-10-30 – 2017-09-30 Engineer, Department of Catalysis, Center for Physical Sciences and Technology

2012 Technician, Department of Catalysis, Center for Physical Sciences and Technology

Participation in scientific projects 2010-08-02 – 2011-12-31 “New materials for fuel cells: synthesis, characterization and properties” (PI: Dr.

L. Tamašauskaitė-Tamašiūnaitė, reg. No. ATE-10009)

2012-05-02 – 2014-12-31 “New nanostructured materials for fuel cells” (PI: Dr. L. Tamašauskaitė-Tamašiūnaitė, reg. Nr. ATE-12014)

2015-09-16 – 2016-12-31 “Inovative catalytic materials for monopropellant fuel systems of microsattellites“ (PI: Prof. habil dr. E. Norkus, reg. Nr. TEC-15077)

2016-09-01 – 2018-08-31 “Wood-based Carbon Catalysts for Low-temperature Fuel Cells (WoBaCat)“ (PI. dr. L. Tamašauskaitė Tamašiūnaitė, reg. No. project3213)

NOTES

NOTES

Vilniaus universiteto leidykla
Universiteto g. 1, LT-01513 Vilnius
El. p. info@leidykla.vu.lt,
www.leidykla.vu.lt
Tiražas 30 egz.